

**Rafael da Silva Raqueti**

**On the Calibration of Bouc-Wen Model  
to Describe the Viscoelasticity in Steady-State Rolling Tires**

Ilha Solteira

2022

UNIVERSIDADE ESTADUAL PAULISTA “JÚLIO DE MESQUITA FILHO”  
FACULDADE DE ENGENHARIA  
CAMPUS DE ILHA SOLTEIRA

**Rafael da Silva Raqueti**

**On the Calibration of Bouc-Wen Model  
to Describe the Viscoelasticity in Steady-State Rolling Tires**

A dissertation submitted to the Faculdade de Engenharia de Ilha Solteira - UNESP as a part of the requirements for obtaining the Master's degree in Mechanical Engineering.

Knowledge area: Solid Mechanics

Advisor: Prof. Dr. Samuel da Silva

Ilha Solteira

2022

FICHA CATALOGRÁFICA

Desenvolvido pelo Serviço Técnico de Biblioteca e Documentação

R221c Raqueti, Rafael da Silva.  
On the calibration of Bouc-Wen model to describe the viscoelasticity in steady-state rolling tires / Rafael da Silva Raqueti. -- Ilha Solteira: [s.n.], 2022  
67 f. : il.

Dissertação (mestrado) - Universidade Estadual Paulista. Faculdade de Engenharia de Ilha Solteira. Área de conhecimento: Mecânica dos Sólidos, 2022

Orientador: Samuel da Silva  
Inclui bibliografia

1. Calibração de modelos. 2. Histerese. 3. Modelo de Bouc-Wen. 4. Viscoelasticidade.

  
Raiane da Silva Santos

**CERTIFICADO DE APROVAÇÃO**

**TÍTULO DA DISSERTAÇÃO: On the Calibration of Bouc-Wen model to describe the viscoelasticity in steady-state rolling tires**

**AUTOR: RAFAEL DA SILVA RAQUETI**

**ORIENTADOR: SAMUEL DA SILVA**

Aprovado como parte das exigências para obtenção do Título de Mestre em ENGENHARIA MECÂNICA, área: Mecânica dos Sólidos pela Comissão Examinadora:

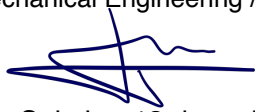


Prof. Dr. SAMUEL DA SILVA (Participação Virtual)  
Departamento de Engenharia Mecânica / Faculdade de Engenharia de Ilha Solteira - UNESP



Prof. Dr. AMERICO BARBOSA DA CUNHA JUNIOR (Participação Virtual)  
Instituto de Matemática e Estatística / Universidade do Estado do Rio de Janeiro - UERJ

Prof. Dr. JEAN-FRANÇOIS DEÛ (Participação Virtual)  
Mechanical Engineering / Conservatoire national des arts et métiers (Cnam), Paris



Ilha Solteira, 13 de maio de 2022

## **Acknowledgments**

First of all, I am grateful to God for being able to complete this work.

Second, I am grateful to my family and friends for all the support and help. To my parents Aparecida and Mario, and to my sister Gabriela. I would like to thank my friend Rafael de O. Teloli for all his help during the realization of this work.

Third, I would like to thank my advisor Prof. Dr. Samuel da Silva for all the advice, and the opportunities throughout my academic studies.

Fourth, I am grateful to Michelin for providing and entrusting us with the dataset to be used in this work. In particular, I would like to thank Philippe Bussetta, a scientific researcher at Michelin. I am also grateful for the financial support provided by the Coordination for the Improvement of Higher Education Personnel (CAPES) Grant No. 88887.583012/2020-00.

## Abstract

Reducing tire rolling resistance and energy loss is a topic of interest to the tire industry. Understanding and modeling these phenomena are essential to approach this problem and propose robust solutions. This work suggests a model based on the Bouc-Wen model to simulate internal variables from viscoelastic constitutive laws. Furthermore, sensitivity analysis is performed on the Bouc-Wen model parameters to evaluate their influence on the system response and capture the full range of possible values that improve the predictive ability of the suggested model. This task calculates the Sobol' indices estimated from a Polynomial-Chaos expansion based on the Bouc-Wen parameters. Once the range of feasible model solutions is established, the proposed model is calibrated through Bayesian inference. Finally, the uncertainties are propagated, and the model is validated using data of viscoelastic internal variables from the finite element approximation of a steady-rolling tire provided by Michelin. Satisfactory results are obtained, as the proposed model can simulate viscoelastic internal variables with a reduced computational cost for some branches of interest. Its outputs are in agreement with the finite element approximation data.

**Keywords:** viscoelastic internal variables; hysteresis; Bouc-Wen model; Sobol' indices; Bayesian inference; propagation of uncertainties.

## Resumo

Reduzir a resistência ao rolamento e as perdas de energia em pneus é um tema de interesse industrial. Compreender e modelar esses fenômenos são essenciais para abordar esse problema e propor soluções robustas. Este trabalho sugere um modelo baseado no modelo de Bouc-Wen para simular variáveis internas a partir de leis constitutivas viscoelásticas. Além disso, a análise de sensibilidade é realizada nos parâmetros do modelo Bouc-Wen para avaliar sua influência na resposta do sistema e também capturar toda a gama de valores viáveis que melhoram a capacidade preditiva do modelo sugerido. Esta tarefa é realizada calculando os índices de Sobol estimados a partir de uma expansão em Caos Polinomial com base nos parâmetros de Bouc-Wen. Uma vez estabelecida a gama de soluções viáveis do modelo, o modelo proposto é calibrado através da inferência Bayesiana. Finalmente, as incertezas são propagadas e o modelo é validado usando dados de variáveis internas viscoelásticas da aproximação por elementos finitos de um pneu em rolamento em contato contínuo fornecido pela Michelin. Resultados satisfatórios são obtidos, pois o modelo proposto pode simular as variáveis internas viscoelásticas com custo computacional reduzido para alguns ramos de interesse e suas respostas estão de acordo com os dados da aproximação por elementos finitos.

**Palavras-chave:** variáveis internas viscoelásticas; histerese; modelo de Bouc-Wen; índices de Sobol; inferência bayesiana; propagação de incertezas.

## List of Figures

1	Generalized Maxwell model. . . . .	20
2	Examples of the components of the right Cauchy-Green tensor from the dataset. . . . .	21
3	Corresponding viscoelastic internal variables for Maxwell branches 1, 4, 5 and 10 from the dataset. There is no dynamic behavior in the higher branches.	22
4	The complete model is defined containing the first 4 Maxwell branches of the generalized Maxwell model. Branches of interest: Branch 1, 2, 3 and 4.	23
5	Examples of hysteresis loops in Branch 1. The Bouc-Wen model is considered to model the hysteretic behavior between the components of the right Cauchy-Green deformation tensor and viscoelastic internal variables. . . . .	23
6	An overview of the calibration strategy: Global sensitivity analysis by valuating the Sobol' indices; Optimization through the Cross-Entropy method; Bayesian inference to estimate the parameters distributions; Propagation of uncertainties. . . . .	27
7	A schematic of the different steps in this work, including the model calibration strategy. . . . .	38
8	A recall of the complete model. Branches of interest: Branches 1, 2, 3 and 4.	39
9	Branch 1, Group 1 – Comparison between error metrics $\bar{E}(\boldsymbol{\theta})$ and $\tilde{E}(\boldsymbol{\theta})$ . The disposition of the 100 cross-validation samples + indicates that the PCE-based surrogate model is adequate. . . . .	41
10	Branch 1, Group 1 – Prior global sensitivity analysis. Total and first-order Sobol' indices of parameters $\gamma$ and $\delta$ are negligible. Therefore, $\gamma$ and $\delta$ can be considered as completely determined quantities. . . . .	41
11	Comparison between Sobol' indices based on Monte Carlo estimation and polynomial chaos expansion. . . . .	42
12	Branch 1, Group 1 – Bayesian inference. Convergence study of parameter $c$ : first (Mean) and second central moments (Variance). The acceptance rate is $\bar{a} \approx 43\%$ and no burn-in samples were considered. . . . .	44
13	Branch 1, Group 1 – Bayesian inference. Convergence study of parameter $k$ : first (Mean) and second central moments (Variance). The acceptance rate is $\bar{a} \approx 43\%$ and no burn-in samples were considered. . . . .	44



14	Branch 1, Group 1 – Bayesian inference. Convergence study of parameter $\alpha$ : first (Mean) and second central moments (Variance). The acceptance rate is $\bar{a} \approx 43\%$ and no burn-in samples were considered. . . . .	45
15	Branch 1, Group 1 – Bayesian inference. Convergence study of parameter $\nu$ : first (Mean) and second central moments (Variance). The acceptance rate is $\bar{a} \approx 43\%$ and no burn-in samples were considered. Number of samples to reach convergence is $2 \times 10^4$ samples (indicated by the magenta vertical line). . . . .	45
16	Branch 1, Group 1 – Bayesian inference. Convergence study of the variance of the discrepancy: first (Mean) and second central moments (Variance). The acceptance rate is $\bar{a} \approx 43\%$ and no burn-in samples were considered. . . . .	46
17	Branch 1, Group 1 – Bayesian inference. Trace plots of the parameters of the Bouc-Wen model and the variance of the discrepancy: the samples were generated using different random number generator seeds. . . . .	47
18	Branch 1, Group 1 – Bayesian inference. Distributions of the parameters of the Bouc-Wen model and variance of the discrepancy: Uniform prior (Prior), estimated probability density functions (EPDF) and empirical cumulative distribution functions (ECDF). . . . .	48
19	Branch 1, Group 1 - Convergence study of the error metric: first (Mean) and second central moments (Variance). . . . .	49
20	Branch 1 - Distributions of the error metric: estimated probability density function (EPDF) and empirical cumulative distribution function (ECDF). The minimum values given by the CE method are $\hat{E} = 0.3171$ (Group 1) and $\hat{E} = 0.3655$ (Group 2). . . . .	50
21	Branch 2 – Distributions of the error metric: estimated probability density function (EPDF) and empirical cumulative distribution function (ECDF). The minimum values given by the CE method are $\hat{E} = 0.3942$ (Group 1) and $\hat{E} = 0.4347$ (Group 2). . . . .	50
22	Branch 3 – Distribution of the error metric: estimated probability density function (EPDF) and empirical cumulative distribution function (ECDF). The minimum values given by the CE method are $\hat{E} = 0.5776$ (Group 1) and $\hat{E} = 0.6857$ (Group 2). . . . .	51
23	Branch 4 – Distribution of the error metric: estimated probability density function (EPDF) and empirical cumulative distribution function (ECDF). The minimum values given by the CE method are $\hat{E} = 1.0116$ (Group 1) and $\hat{E} = 1.6672$ (Group 2). . . . .	51

24	Branch 1, Group 1 – Propagation of the uncertainties. Responses of the stochastic model: 95% confidence interval (CI), its mean (Mean) and corresponding viscoelastic internal variables from the dataset ( $A^{\text{DS}}$ ). Best Group 1 estimation scenario. . . . .	52
25	Branch 4, Group 1 – Propagation of the uncertainties. Responses of the stochastic model: 95% confidence interval (CI), its mean (Mean) and corresponding viscoelastic internal variables from the dataset ( $A^{\text{DS}}$ ). Worst Group 1 estimation scenario. . . . .	53
26	Branch 1, Group 1 – Deterministic responses of the Bouc-Wen model: CE method, MAP and corresponding viscoelastic internal variables from the dataset ( $A^{\text{DS}}$ ). . . . .	56
27	Branch 4, Group 1 – Deterministic responses of the Bouc-Wen model: CE method, MAP and corresponding viscoelastic internal variables from the dataset ( $A^{\text{DS}}$ ). . . . .	57
28	Bayesian inference using a PCE-based surrogate model. Branch 1, Group 1 – Comparison between error metrics $\bar{E}(\boldsymbol{\theta})$ and $\tilde{E}(\boldsymbol{\theta})$ . The disposition of the 100 cross-validation samples + indicates that the PCE-based surrogate model was adequate. . . . .	58
29	Bayesian inference using a PCE-based surrogate model. Branch 1, Group 1 – Distributions of the parameters of the Bouc-Wen model and variance of the discrepancy parameter: Uniform prior (Prior), estimated probability density functions (EPDF) and empirical cumulative distribution functions (ECDF). . . . .	60

## List of Tables

1	Uniform distributions of the parameters of the Bouc-Wen model used in the prior global sensitivity analysis. . . . .	40
2	Information about the PCE-based surrogate model. . . . .	40
3	Branch 1 – Cross-Entropy method. Elapsed time and optimal values of the influential parameters of the Bouc-Wen model. . . . .	43
4	Branches 1, 2 and 3 – Bayesian inference. Uniform prior distribution of the parameters of the Bouc-Wen model and the variance of the discrepancy. . .	43
5	Branch 4 – Bayesian inference. Uniform prior distribution of the parameters of the Bouc-Wen model and the variance of the discrepancy. . . . .	43
6	Branch 1, Group 1 - Bayesian inference. Elapsed time to estimate the values of the parameters of the Bouc-Wen model and the variance of the discrepancy. $N_k = 2 \times 10^4$ samples. . . . .	46
7	Cross-Entropy method. Elapsed time to estimate the values of the parameters of the Bouc-Wen model: $N_s = 100$ samples, $N_{\mathcal{E}} = 4$ samples, $\epsilon_{\max} = 10^{-6}$ , $l_{\max} = 500$ iterations and $a = 0.8$ . . . . .	54
8	Bayesian inference. Elapsed time to estimate the values of the parameters of the Bouc-Wen model and the variance of the discrepancy: $N_k = 2 \times 10^4$ samples. . . . .	54
9	Estimated values of the parameters of the Bouc-Wen model and the variance of the discrepancy. . . . .	55
10	Bayesian inference using a PCE-based surrogate model. Validation of the PCE-based surrogate model. . . . .	58

## List of Acronyms

BW	Bouc-Wen
CE	Cross-Entropy
CI	Confidence interval
DE	Differential equation
FEM	Finite element method
GMM	Generalized Maxwell model
GSA	Global sensitivity analysis
IC	Initial condition
MASE	Mean absolute scaled error
MaxEnt	Maximum entropy
ODE	Ordinary differential equation
PCE	Polynomial chaos expansion
PDE	Partial differential equation
ROM	Reduced-order model

## List of Symbols

$C$	Component of the right Cauchy-Green tensor
$C^{\text{DS}}$	Component of the right Cauchy-Green tensor from the dataset
$A$	Viscoelastic internal variable
$A^{\text{DS}}$	Viscoelastic internal variable from the dataset
$t$	Time
$c$	Damping coefficient
$k$	Elasticity coefficient

$A(t, \boldsymbol{\theta})$	Bouc-Wen model response of viscoelastic internal variable
$\dot{A}(t, \boldsymbol{\theta})$	Bouc-Wen model response of viscoelastic internal variable time derivative
$A_0$	Bouc-Wen model response of viscoelastic internal initial condition
$\mathcal{Z}(t, \boldsymbol{\theta}, A, \dot{A})$	Bouc-Wen model response of hysteretic output
$\dot{\mathcal{Z}}(t, \boldsymbol{\theta}, A, \dot{A})$	Bouc-Wen model response of hysteretic output time derivative
$\mathcal{Z}_0$	Bouc-Wen model response of hysteretic output initial condition
$E(\boldsymbol{\theta})$	Mean absolute scaled error response
$\bar{E}(\boldsymbol{\theta})$	Mean of MASE responses, error measure
$\hat{E}$	Optimal error measure value
$\mathbf{X}$	Random input vector
$\mathcal{M}$	Mathematical model
$Y$	Output of interest
$S_i$	First-order Sobol' indices
$S_{ij}$	Second-order Sobol' indices
$y_\alpha$	PCE coefficients
$\mathcal{A}$	Truncation criterion
$\mathcal{B}$	Feasible region
$N_s$	Number of samples
$N_{\mathcal{E}}$	Number of elite samples
$l_{\max}$	Maximum of iteration level
$a$	Smooth updating schema parameter
$\boldsymbol{x}$	Set of parameters considering the variance of the discrepancy parameter
$N_k$	Number of samples in the Markov chain
$N_a$	Number of accepted samples
$\bar{a}$	Acceptance rate

## Greek Letters

$\alpha$	Parameter of the Bouc-Wen model
----------	---------------------------------

$\gamma$	Parameter of the Bouc-Wen model
$\delta$	Parameter of the Bouc-Wen model
$\nu$	Parameter of the Bouc-Wen model
$\boldsymbol{\theta}$	Set of parameters of the Bouc-Wen model
$\hat{\boldsymbol{\theta}}$	Optimal set of parameters of the Bouc-Wen model value
$\varphi_\alpha$	Multivariate polynomials
$\epsilon_{\max}$	Stopping criterion
$\sigma_\epsilon^2$	Variance of the discrepancy parameter
$\pi(\boldsymbol{x})$	Prior distribution of parameters
$\pi(\boldsymbol{x} \bar{E}(\boldsymbol{\theta}))$	Posterior distribution of parameters
$\sigma^2$	Random walk step size

# Contents

MOTIVATION . . . . .	
OBJECTIVES . . . . .	
MAIN CONTRIBUTIONS . . . . .	
OUTLINE . . . . .	
<b>1 BOUC-WEN MODEL</b>	<b>19</b>
1.1 THE COMPLETE MODEL . . . . .	19
1.1.1 Michelin's dataset . . . . .	21
1.2 THE BOUC-WEN MODEL . . . . .	24
1.3 A data selection procedure . . . . .	25
1.4 CONCLUDING REMARKS . . . . .	26
<b>2 A MODEL CALIBRATION STRATEGY</b>	<b>27</b>
2.1 ERROR METRIC DEFINITION . . . . .	28
2.2 GLOBAL SENSITIVITY ANALYSIS . . . . .	29
2.2.1 Sobol' indices . . . . .	29
2.2.2 Polynomial-Chaos expansion . . . . .	30
2.3 THE CROSS-ENTROPY METHOD . . . . .	31
2.4 BAYESIAN INFERENCE . . . . .	34
2.4.1 Markov chain Monte Carlo . . . . .	35
2.5 CONCLUDING REMARKS . . . . .	37
<b>3 RESULTS AND DISCUSSION</b>	<b>39</b>
3.1 BOUC-WEN MODEL CALIBRATION . . . . .	40
3.2 PCE-BASED SURROGATE MODEL CALIBRATION . . . . .	58
<b>4 FINAL REMARKS</b>	<b>61</b>
4.1 SUMMARY . . . . .	61
4.2 PERSPECTIVES OF FUTURE WORK . . . . .	62
4.3 CONTRIBUTIONS TO THE LITERATURE . . . . .	64
<b>REFERENCES</b>	<b>65</b>

## MOTIVATION

Due to the rise of a sustainability mindset in businesses, state regulations, and consumer requirements, the automobile industry has sought to develop technologies to improve vehicle performance, minimize fuel consumption, and reduce pollutant emissions. Nowadays, improving sustainable practices in both academic and productive sectors is more necessary to reduce environmental impacts. In the same way, with the expansion of the electric vehicle fleet, the generation of particulate matter by vehicle parts such as brakes and tires has become important (OROUMIYEH; ZHU, 2021; TONEGAWA; SASAKI, 2021). In both contexts, improving tire performance is desirable.

In a rolling tire, the mechanisms of energy loss have been known for a long time: the friction inherent in the contact between the tire and the road, the drag force of the air, and the hysteresis within the viscoelastic material (WALTER; CONANT, 1974). These energy loss mechanisms contribute to the rolling resistance, which can be considered a force that opposes the vehicle's movement. The rolling resistance is responsible for a significant amount of energy consumption (HALL; MORELAND, 2001), and most of it results from hysteretic loss. This loss is influenced by the characteristics of the tire, such as its dimensions and material, and by external variables such as the vehicle speed, wheel load, and inflation pressure (WALTER; CONANT, 1974). The tire industry is still working on new solutions to reduce the rolling resistance and improve tire performance simultaneously, e.g., by improving handling, grip, comfort, and durability and reducing the wearing noise. To achieve this goal, it is necessary to design new tires and change the variables that affect the rolling resistance. However, there is no point in doing a few tests for each new tire design. Hence, the importance of modeling a tire. Moreover, some of these variables are uncertain, and a robust model could help investigate how the uncertainties in tire properties affect rolling resistance.

There are several approaches to model a tire in the literature: from experimental data only, using similarity methods, or through physical models (PACEJKA, 2012). These approaches are different in accuracy and complexity. Among them, the finite element method considers material and physical complexities and is commonly adopted by the tire industry for modeling rolling tires (GHOREYSHI, 2008). In a steady-state rolling tire, the finite element approximation depends on the viscoelasticity. Viscoelasticity can be described by a set of constitutive laws, which are a function of internal variables. Nonlinear differential equations govern the evolution of internal variables (TALLEC; RAHLER, 1994). It is still challenging to characterize the viscoelastic material considering its complexities, such as time-varying properties and energy dissipation. Despite the good accuracy of the results, the finite element method becomes time-consuming when these complexities are considered. Furthermore, the high computational cost motivates the investigation of alternative



modeling methods, e.g., an analytical model was developed based on a hysteresis model to quantify the dissipated energy (BRANCATI; STRANO; TIMPONE, 2011).

Due to the model complexity and the presence of nonlinearities in structural dynamics problems such as the viscoelasticity in a steady-rolling tire, it is worth analyzing the construction of reduced-order models. A reduced-order model is an alternative to a defined full-order model. Its advantage is to reduce computational cost while retaining model accuracy (SULLIVAN; YAMASHITA; SUGIYAMA, 2022). Unlike the surrogate models based on the definition of a response surface (ALIZADEH; ALLEN; MISTREE, 2020), the reduced-order model is based on physical simplifications of the full-order model and depends on parameters that translate these simplifications. Doing so reduces the computational time, and some physical aspects of the complete model are preserved. In the same context, the present work is motivated by the progress in the field of simple models applied to steady-state rolling tire problems. To get around the description of nonlinearities using a finite element model, as is commonly done in the tire industry, an alternative model is suggested to simulate the viscoelastic internal variables. Such a model can be constructed from a complex model consisting of a set of constitutive equations that describes the viscoelasticity in the finite element approximation. In addition, the hysteresis within the viscoelastic material can be an alternative for constructing this alternative model. To describe the viscoelasticity by solving a less computationally expensive model with minor loss of information, the parameters of the suggested model can be inferred thanks to a dataset provided by Michelin for this work.

## OBJECTIVES

Generally speaking, this work proposes a set of models to simulate the viscoelastic internal variables that describe the behavior of steady-state rolling tires. For this purpose, the following objectives are defined:

- To formulate a model based on the set of constitutive laws governing the incompressible viscoelastic material and the hysteresis;
- To implement a model calibration procedure using data generated during the computation of a finite element approximation of steady-state rolling tire.

This work also aims to contribute to the alternative treatment of the nonlinearities inherent to the modeling of the viscoelastic material: the viscoelastic internal variables are computed by less computationally expensive and suitably accurate models compared to the finite element approximation.

## MAIN CONTRIBUTIONS

The main contributions of this work are:

- The formulation of a model to simulate viscoelastic internal variables based on the generalized Maxwell and Bouc-Wen models;
- The determination of the influential parameters of the Bouc-Wen model through global sensitivity analysis. The global sensitivity analysis is performed by evaluating the Sobol' indices from a surrogate model based on Polynomial-Chaos expansion;
- The implementation of a model calibration strategy combining optimization and statistical inference techniques: an optimization problem is solved by the Cross-Entropy method, and the influential parameters are further estimated using Bayesian inference;
- The propagation of the uncertainties of the proposed model parameters through the responses.

## OUTLINE

This work is organized into the following chapters:

- **Chapter 1 - BOUC-WEN MODEL** initially relates the complete model and Michelin's dataset to the Bouc-Wen model through the hysteresis phenomenon. Then, from this relation, this chapter formulates the proposed model;
- **Chapter 2 - A MODEL CALIBRATION STRATEGY** describes the implemented model calibration strategy: initially, this chapter defines an error metric; then, it describes global sensitivity analysis, Sobol' indices, and Polynomial-Chaos expansion; likewise, this chapter describes the Cross-Entropy method and Bayesian inference;
- **Chapter 3 - RESULTS AND DISCUSSION** critically discusses the results obtained from the calibration of the set of proposed models;
- **Chapter 4 - FINAL REMARKS** presents the conclusion and suggests directions to further advance this research.

# 1 BOUC-WEN MODEL

This chapter details the development of the suggested model. To this end, part of a finite element model is addressed first. Next, a data selection procedure is defined. Then, the suggested model is then formulated based on hysteresis.

---

## 1.1 THE COMPLETE MODEL

First of all, it is important to stress that the complete development of the finite element model of the tire under analysis is beyond the scope of this work. Confidentiality terms protect further details about the material properties, dimensions, and geometry. The elapsed time for evaluating the finite element model is also unknown. Nevertheless, this section is intended to provide information about the dataset generated from the covered finite element model. From this information, it is expected to address the complete model and detail the basis of the suggested model formulation.

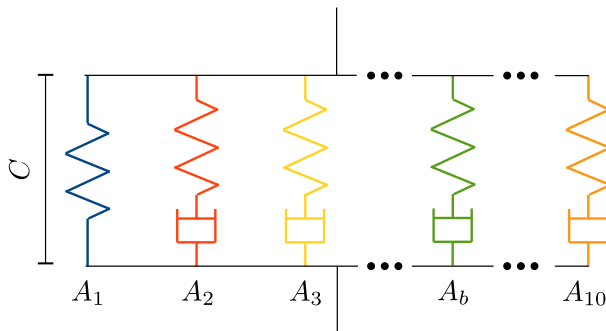
The dataset is generated during the computation of a finite element approximation of a steady-state rolling tire. This approximation couples the constitutive laws governing the behavior of the incompressible viscoelastic material behavior and the equilibrium equations governing the steady-state rolling motion (TALLEC; RAHLER, 1994). A standard finite element procedure is adopted to approximate this problem. It is worth noting that the finite element method is widely adopted by the tire industry for modeling steady-state rolling tires (GHOREYSHI, 2008). In addition, a finite element model can take into account different physical complexities: a finite element approximation can couple the Kelvin-Voigt rheological model and an axisymmetric body in a 2D analysis (TALLEC; RAHLER, 1994); or the Mooney-Rivlin model and more complex tire model in a 3D analysis (LIU; HOFSTETTER; MANG, 1994). The more reliable the approximation, the more accurate the model responses. However, physical complexities such as the internal variables influence the computational cost.

During the standard finite element procedure, convenient choices of internal variables must be made because nonlinear differential equations govern their dynamic behavior. Assuming a general formulation, the elastic and viscous potentials that compose the constitutive laws could be derived from a generalized Kelvin-Maxwell model (FANCELLO; PONTHOT; STAINIER, 2006). Or else, the viscoelasticity could be described by choos-

ing a specific free energy potential that is a function of the states variables: temperature, right Cauchy-Green deformation tensor, and viscoelastic internal variables (TALLEC; RAHLER, 1994). The dataset covered here consists of data of the components of the right Cauchy-Green deformation tensor and viscoelastic internal variables from a generalized Maxwell model. The generalized Maxwell model describes the viscoelastic internal variables at the nodes of the finite element approximation of the tire. The viscoelastic internal variables are rank 2 symmetric positive-definite tensors (TALLEC; RAHLER, 1994).

The theoretical representation of the generalized Maxwell model consists of the parallel association of several Maxwell branches. Each Maxwell branch consists of a series association of elastic and viscous elements. Figure 1 is a representation of the rheological model, in which  $C$  is a component of the right Cauchy-Green tensor and  $A_b$  the viscoelastic internal variable at the Maxwell branch  $b$ . The complete rheological model contains 10 Maxwell branches.

Figure 1: Generalized Maxwell model.



Source: Author's own elaboration.

A component  $C$  of the right Cauchy-Green deformation tensor affects each one of the Maxwell branches in Figure 1. How a particular branch responds depends on its properties. The dynamic behavior of the viscoelastic internal variable  $A_b$  is expected to be a function of the elastic and viscous elements of the Maxwell branch  $b$ . Assuming that the elastic element is described by a coefficient of elasticity coefficient  $k_b$  and the viscous element by a damping coefficient  $c_b$ , a model candidate could be:

$$C(t) = k_b A_b(t) + c_b \dot{A}_b(t). \quad (1)$$

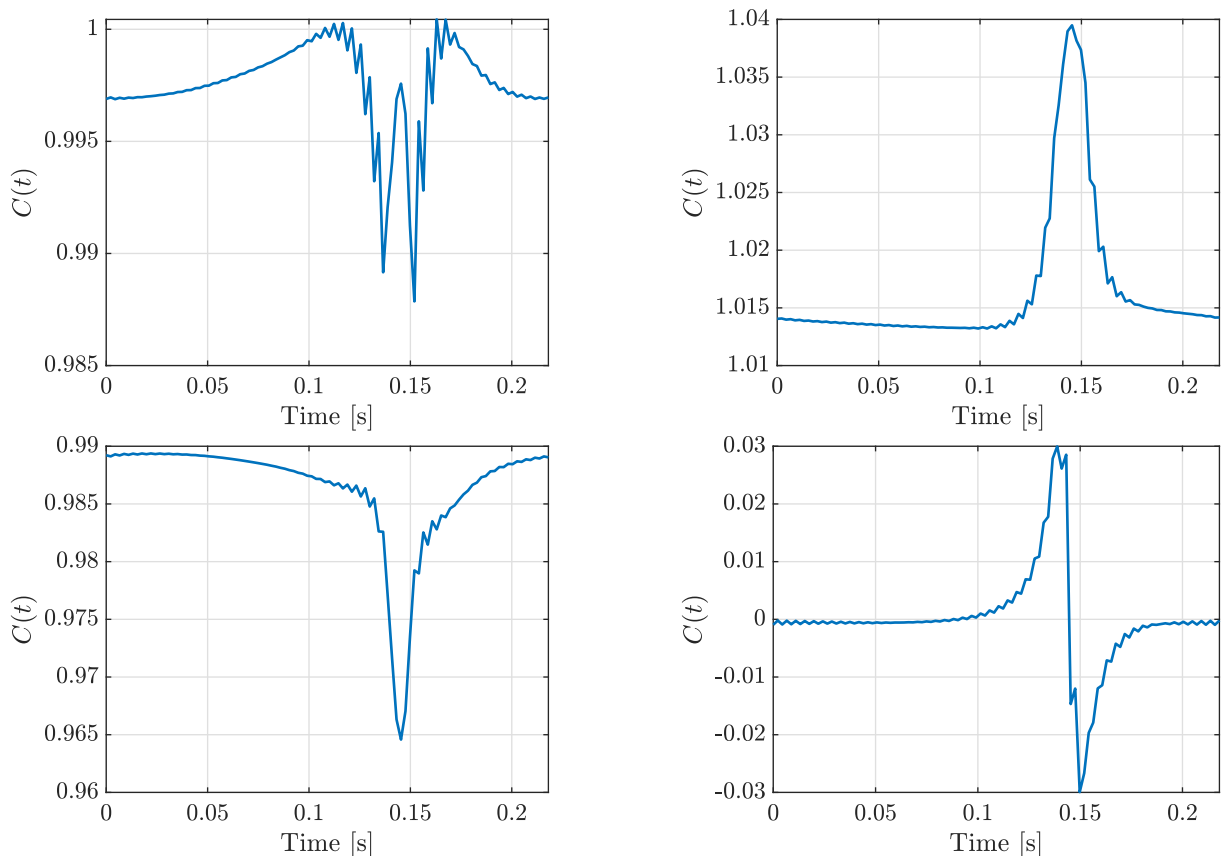
However, this formulation does not consider nonlinear effects such as the hysteresis loop examples that are presented later in Figure 5. Looking for new information that can be used to formulate a simple model, it is interesting to observe the dynamic behavior of the variables  $C(t)$  and  $A_b(t)$  through the dataset.

### 1.1.1 Michelin's dataset

To conduct this work, Michelin provided a dataset composed of many components  $C$  of the right Cauchy-Green deformation tensor and the respective viscoelastic internal variables  $A$  in all Maxwell branches of Figure 1. Overall, the dataset contains 96 components of the right Cauchy-Green deformation tensor, structured in 16 tensors of 6 components each.

Some observations can be made from the examples of components of the right Cauchy-Green tensor in Figure 2. The first one is the cyclic motion of the tire: a node describes a complete revolution in just over 0.2 seconds. Then, it returns to its initial condition. The second one is the contact between the tire and the soil: between 0.1 and 0.2 seconds, there are significant variations in  $C$ . The dynamic behavior in this interval characterizes the passage of a node through the contact region.

Figure 2: Examples of the components of the right Cauchy-Green tensor from the dataset.

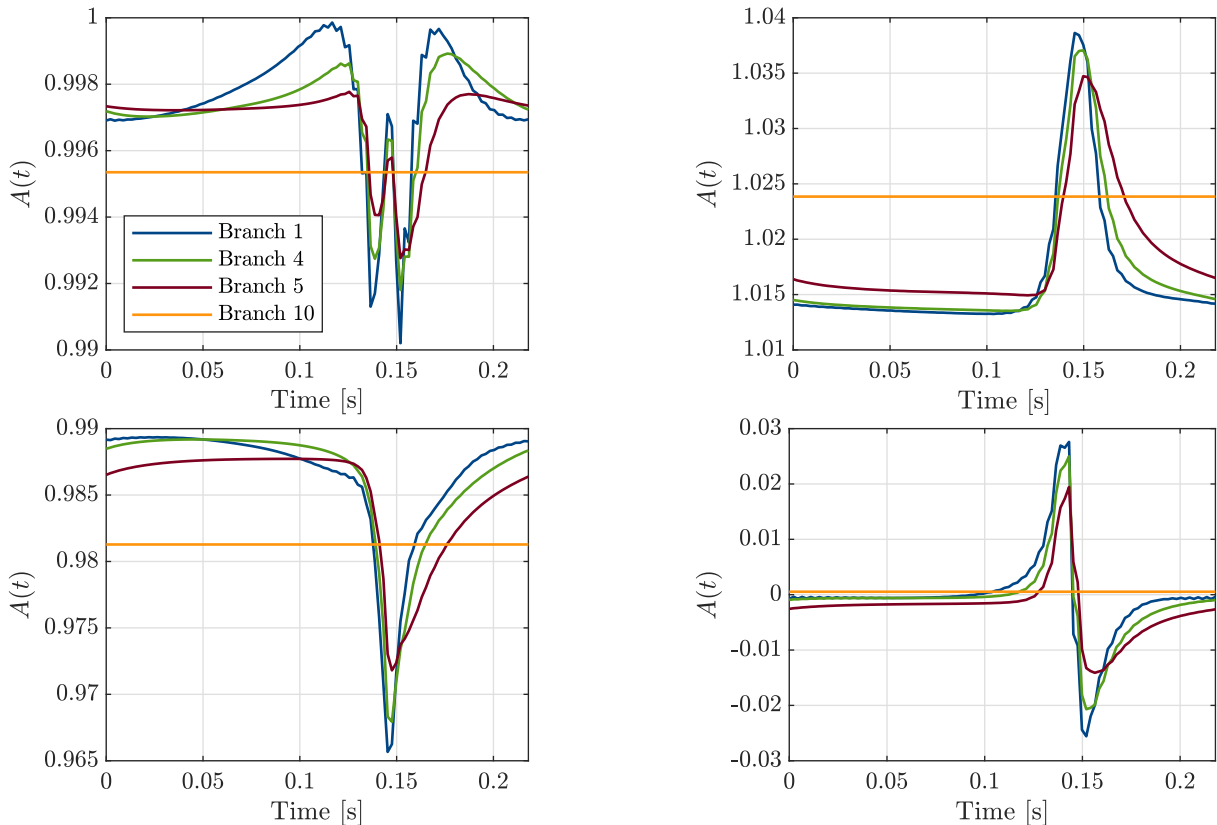


Source: Author's own elaboration.

As stated earlier, each of these components affects the Maxwell branches of the generalized Maxwell model in Figure 1. Figure 3 shows the corresponding viscoelastic internal variables for Maxwell branches 1, 4, 5 and 10. This figure shows that the viscoelastic internal variables attenuate in the higher branches until there is no dynamic behavior

in Maxwell branch 10. However, the present work proposes to simulate the viscoelastic internal variables that exhibit dynamic behavior. From this, the branches of interest are defined: Branch 1, 2, 3, and 4. They correspond to the first 4 Maxwell branches in Figure 1. In the sequence, the complete model is simply a cutout of the generalized Maxwell model that contains only the branches of interest, and it is shown in Figure 4.

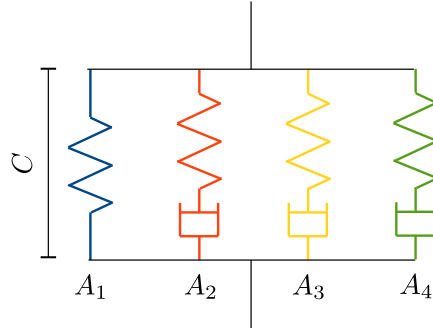
Figure 3: Corresponding viscoelastic internal variables for Maxwell branches 1, 4, 5 and 10 from the dataset. There is no dynamic behavior in the higher branches.



Source: Author's own elaboration.

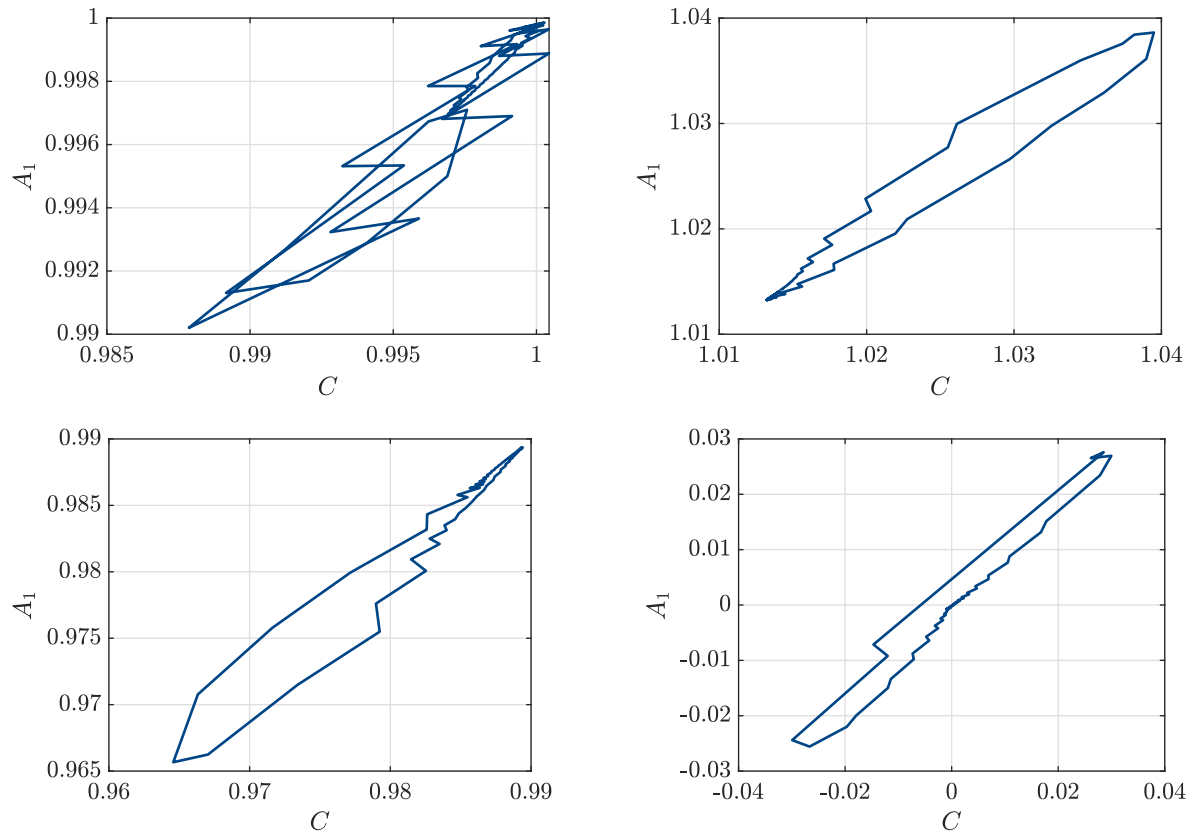
After this reduction in the quantity of data to be analyzed by defining the complete model, it is interesting to observe the behavior of the components of the right Cauchy-Green deformation tensor in the function of the viscoelastic internal variables. Considering only the Branch 1, Figure 5 shows the hysteretic behavior between them. Complementing Equation 1, the following section formulates the suggested model by adding a hysteresis model.

Figure 4: The complete model is defined containing the first 4 Maxwell branches of the generalized Maxwell model. Branches of interest: Branch 1, 2, 3 and 4.



Source: Author's own elaboration.

Figure 5: Examples of hysteresis loops in Branch 1. The Bouc-Wen model is considered to model the hysteretic behavior between the components of the right Cauchy-Green deformation tensor and viscoelastic internal variables.



Source: Author's own elaboration.

## 1.2 THE BOUC-WEN MODEL

For one branch of interest in Figure 4, the component  $C = C(t)$  of the right Cauchy-Green deformation tensor and its corresponding viscoelastic internal variable  $A = A(t)$  are both time series. Complementing Equation 1, it is assumed that  $C(t)$  is the sum of three terms: a linear elastic given by  $k A(t)$  in which  $k$  is a coefficient of elasticity; a viscous  $c \dot{A}(t)$  in which  $c$  is a damping coefficient; and a hysteretic output  $\mathcal{Z}(A, \dot{A})$ :

$$C(t) = k A(t) + c \dot{A}(t) + \mathcal{Z}(A, \dot{A}). \quad (2)$$

The hysteresis phenomenon is recurrent in many areas of science. In dynamic structural systems, the hysteresis occurs as a natural response of the material against the movement. The hysteresis is related to the memory effect of inelastic behavior. It depends not only on the instantaneous deformation but also on its history (ISMAIL; IKHOUANE; RODELLAR, 2009).

Different models can describe the hysteresis. In (BRANCATI; STRANO; TIMPONE, 2011), the Dahl's model is used to model the restoring force-strain relation. The authors proposed a strain-restoring force model corresponding to the sum of linear elastic, viscous and nonlinear hysteretic terms. Instead of using the Dahl's model, the adopted approach in this work is to model the hysteresis with the Bouc-Wen model. The latter can describe different nonlinear dissipation mechanisms through a first-order nonlinear differential equation. The Bouc-Wen model is prevalent in many applications because it can fit real hysteresis loops by choosing the parameters appropriately. That is why the Bouc-Wen model is often related to parameter estimation problems. A survey on the Bouc-wen model can be found in (ISMAIL; IKHOUANE; RODELLAR, 2009). Equation 3 defines the hysteretic output  $\mathcal{Z}(A, \dot{A})$ :

$$\dot{\mathcal{Z}}(A, \dot{A}) = \alpha \dot{A}(t) - \gamma |\dot{A}(t)| |\mathcal{Z}|^{\nu-1} \mathcal{Z} - \delta \dot{A}(t) |\mathcal{Z}|^{\nu}, \quad (3)$$

where  $\alpha$ ,  $\gamma$ ,  $\delta$  and  $\nu$  are the parameters of the Bouc-Wen model. After algebraic manipulation of Equations 2 and 3, the suggested model is defined by the following system of first-order nonlinear differential equations:

$$\begin{cases} \dot{A}(t) = \frac{1}{c} (C(t) - k A(t) - \mathcal{Z}(A, \dot{A})) \\ \dot{\mathcal{Z}} = \alpha \dot{A} - \gamma |\dot{A}| |\mathcal{Z}|^{\nu-1} \mathcal{Z} - \delta \dot{A} |\mathcal{Z}|^{\nu}. \end{cases} \quad (4)$$

In Equation 4, the input  $C(t)$  is completely determined from the dataset<sup>1</sup>. For certain

---

<sup>1</sup>This parameter is assumed to be an input variable in the model and is therefore known for the whole range of analysis



initial conditions  $A|_{t=0} = A_0$  and  $\mathcal{Z}|_{t=0} = \mathcal{Z}_0$ <sup>2</sup>, the output responses  $A(\boldsymbol{\theta})$  and  $\mathcal{Z}$  depend only on the set of parameters  $\boldsymbol{\theta} = \{c, k, \alpha, \gamma, \delta, \nu\}$ . Equation 4 can be solved numerically by a classic Runge-Kutta method.

As for prior knowledge about the parameters, both the damping coefficient  $c$  and the coefficient of elasticity  $k$  are strictly positive. It is worth noting that the Bouc-Wen model is a phenomenological model:  $\alpha$ ,  $\gamma$ ,  $\delta$ , and  $\nu$  do not necessarily have a physical meaning. Some conditions on the Bouc-Wen model parameters are indicated for physical and mathematical consistency in (ISMAIL; IKHOUANE; RODELLAR, 2009), e.g., the Bouc-Wen model fulfills the second law of Thermodynamics if and only if  $\nu > 0$ ,  $\gamma > 0$  and  $-\gamma \leq \delta \leq \gamma$ . Moreover, the Bouc-Wen model is bounded input-bounded output stable and consistent with the motion of physical systems if  $\alpha > 0$ ,  $\gamma + \delta > 0$  and  $\gamma - \delta \geq 0$ . To ensure model consistency, such parameter conditions are adopted in the calibration strategy. Chapter 2 presents an overview of the methods that are combined to infer such parameters.

### 1.3 A data selection procedure

It is essential to highlight that, while the 96 (16 times 6) components of right Cauchy-Green deformation from the dataset are the same for all branches, each branch of the complete model will respond internally in a different way. For a single branch of the complete model in Figure 4, there are 16 right Cauchy-Green deformation tensors. Each right Cauchy-Green deformation tensor has 6 components. Similarly, for the same branch, there are 16 viscoelastic internal variables. The viscoelastic internal variables are rank 2 symmetric positive-definite tensors, and each one has 6 components.

A component of the right Cauchy-Green deformation tensor is a time series. This component may be different from the others (maxima and minima values, derivatives, etc.) as shown in the examples in Figure 2. Similarly, the respective viscoelastic internal variable is also a time series, and one may be different from the others. A hysteresis loop is described by this component of the right Cauchy-Green deformation tensor and the respective viscoelastic internal variable. Therefore, in the dataset, there are 96 (16 times 6) hysteresis loops per branch in the complete model. To be rigorous, each branch would comprise 96 models to simulate all possible viscoelastic internal variables.

There are similar components of the right Cauchy-Green deformation tensor in the dataset. These similarities can be explained by the symmetric construction of the tire approximation used in this work. A selection procedure was defined based on the data

---

<sup>2</sup>In the numerical simulations,  $A_0$  is the first point of the viscoelastic internal variable from the dataset and  $\mathcal{Z}_0 = 0$ .

visualization: different patterns of components of right Cauchy-Green deformation were identified. A single representative from each pattern was retained. After eliminating the redundancies, the number of selected components of the right Cauchy-Green deformation tensor is reduced to 16 inputs. However, instead of 16 models, the calibration strategy defines an error metric that considers the differences in the inputs. The calibration strategy evaluates the parameters of the suggested model in which the error metric is globally minimum. In other words, the suggested model best simulates viscoelastic internal variables considering a reduced number of inputs.

Then, from numerical simulations, it was observed that dividing the inputs into two groups improved performance. The 16 inputs were then visually separated based on patterns between the components of the right Cauchy-Green deformation tensors. For this reason, each branch in Figure 4 can be represented by two different models. Each model is calibrated by considering only 8 inputs.

## 1.4 CONCLUDING REMARKS

The suggested model is a system of first-order nonlinear differential equations that can be solved by a classic Runge-Kutta method. This chapter formulated the suggested model to simulate viscoelastic internal variables to describe the viscoelasticity in steady-state rolling tires. Although the information about the finite element model is limited, the complete model was defined based on a cutout of the generalized Maxwell model. Thanks to the dataset, it was possible to visualize the hysteretic behavior between the components of the right Cauchy-Green tensors and the viscoelastic internal variables. The Bouc-Wen model is able to describe this behavior.

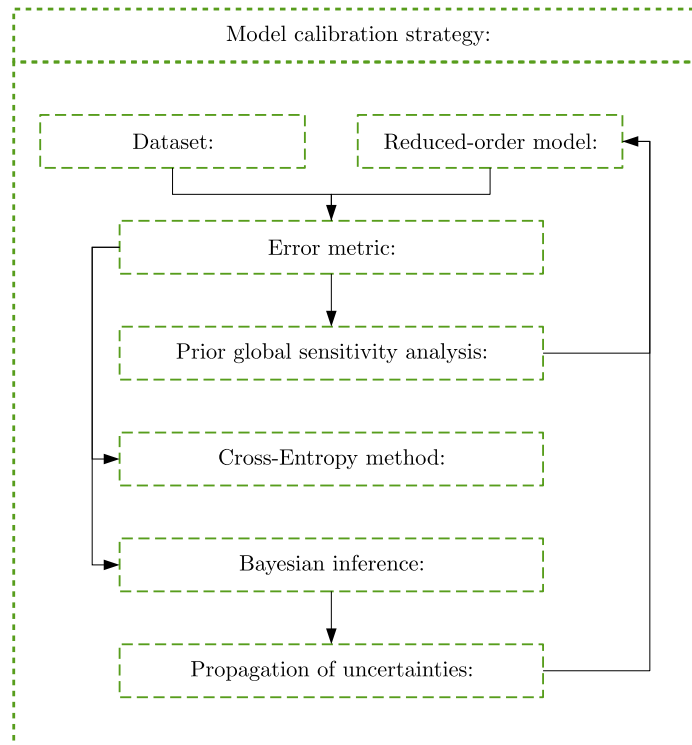
Regarding future steps, some descriptions of this chapter are essential:

1. Through the literature on the Bouc-Wen model, it was possible to get prior knowledge of the parameters of the suggested model. This prior knowledge is essential in the calibration strategy;
2. Observing the dataset's structure allowed the number of inputs to be reduced. In the calibration strategy, this corresponds to a decrease in the computational time required to infer the parameters of the suggested model.

## 2 A MODEL CALIBRATION STRATEGY

This chapter describes the methodology adopted in this work to calibrate the suggested model. To begin, an error metric is defined to evaluate the discrepancy between the suggested model responses and the data. Next, global sensitivity analysis, Sobol's indices, and Polynomial-Chaos expansion are described. The global sensitivity analysis is intended to evaluate the parameters' influence on the error metric's variability. Then, the Cross-Entropy method and Bayesian inference are also described. These methods infer, respectively, the optimal set of parameters and the distributions of the parameters based on the data of viscoelastic internal variables. Finally, the parameter distributions can propagate the uncertainties and extend the suggested model into a stochastic one. Figure 6 shows an overview of the current calibration strategy:

Figure 6: An overview of the calibration strategy: Global sensitivity analysis by valuating the Sobol' indices; Optimization through the Cross-Entropy method; Bayesian inference to estimate the parameters distributions; Propagation of uncertainties.



Source: Author's own elaboration.

## 2.1 ERROR METRIC DEFINITION

As described in the previous chapter, a representative set containing several inputs is selected from the dataset. Due to the formulation of the right Cauchy-Green tensor, the same set is applied to all branches of interest of the full-order model. Into this single set, the inputs differ in maxima and minima values, derivatives, etc. Figure 2 shows different inputs from this set and Figure 5 the respective hysteresis loops in Branch 1. A logical approach is identifying a model for each input in a branch of interest. However, this would substantially increase the complexity of the problem and the number of parameters to be identified. Therefore, the strategy adopted by this work lies in defining a unique model that best forecasts viscoelastic internal variables for a branch of interest considering the whole set of different inputs. To compare the discrepancies between the responses of the suggested model with the internal viscoelastic variables independently of the input differences, the following error metric is defined:

$$E(\boldsymbol{\theta}) = \frac{1}{N_{\text{out}}} \sum_{j=1}^{N_{\text{out}}} \frac{\|A_j^{\text{DS}} - A_j(\boldsymbol{\theta})\|}{\frac{1}{N_{\text{out}}-1} \sum_{j=2}^{N_{\text{out}}} \|A_j^{\text{DS}} - A_{j-1}^{\text{DS}}\|}. \quad (5)$$

Equation 5 is the Mean Absolute Scaled Error (MASE). This error metric evaluates the difference between the response of the suggested model  $A(\boldsymbol{\theta})$  and the viscoelastic internal variable  $A^{\text{DS}}$  from the dataset at  $N_{\text{out}}$  points of the time series. The denominator is a scaling factor that allows us to compare different error metrics independently of the maximum and minimum values of the responses, their derivatives, etc. The MASE is the best available error metric of forecast accuracy in situations with very different scales, including close to zero or negative data (HYNDMAN; KOEHLER, 2006).

Equation 6 is simply the mean between the  $N_{\text{in}}$  evaluations of the error metric  $E_i(\boldsymbol{\theta})$ :

$$\bar{E}(\boldsymbol{\theta}) = \frac{1}{N_{\text{in}}} \sum_{i=1}^{N_{\text{in}}} E_i(\boldsymbol{\theta}). \quad (6)$$

This equation also defines the loss function of an optimization problem, in which  $\hat{\boldsymbol{\theta}}$  is the optimal set of parameters in the set of the feasible solutions  $\mathcal{B}$ :

$$\hat{\boldsymbol{\theta}} = \arg \min_{\mathcal{B}} \bar{E}(\boldsymbol{\theta}), \quad (7)$$

and  $\hat{E} = \bar{E}(\hat{\boldsymbol{\theta}})$  is the minimum error between the suggested model responses and the viscoelastic internal variables from the dataset. It is worth mentioning that other error metrics can be investigated. Alternatively, one can suggest the error metric as a Pearson correlation coefficient with a classical Tikhonov regularization term (DANTAS *et al.*, 2019).

After introducing a metric capable of assessing the performance of the suggested model, the next section introduces the global sensitivity analysis for evaluating the model parameters.

## 2.2 GLOBAL SENSITIVITY ANALYSIS

Global sensitivity analysis refers to a set of mathematical techniques that quantifies input parameters' influence on a system's response of interest. Among other techniques, global sensitivity analysis can be defined by the variance decomposition method, which aims to decompose the output variance as the sum of contributions or combinations of the input variable. Sobol' indices is a variance decomposition method (SOBOL, 1993) that has been recently explored by engineers. Its central idea is to expand a model into the sum of increasing dimension terms and then determine the ratio between the partial variances of these terms and the model's total variance.

### 2.2.1 Sobol' indices

Adopting a generic notation, let  $\mathcal{M}$  be a model and  $\mathbf{X}$  a random input vector gathering  $n$  independent input parameters.  $\mathcal{M}$  describes a scalar output of interest  $Y$  of a physical system:

$$Y = \mathcal{M}(\mathbf{X}), \quad \mathbf{X} = \{X_1, X_2, \dots, X_n\}. \quad (8)$$

$Y$  can also be defined as the sum of increasing dimension terms (SOBOL, 1993). The following description assumes that the input parameters are uniformly distributed and  $\mathcal{D}_{\mathbf{X}} = [0, 1]^n$  is the support of  $\mathbf{X}$ . Therefore,  $Y$  can be written as:

$$Y = \mathcal{M}_0 + \sum_{i=1}^n \mathcal{M}_i(X_i) + \sum_{i<j}^n \mathcal{M}_{ij}(X_i, X_j) + \dots + \mathcal{M}_{1,\dots,n}(X_1, \dots, X_n). \quad (9)$$

The terms of this expansion can be computed through integrals. The first one  $\mathcal{M}_0$  is constant and equal to the expected value:

$$\mathcal{M}_0 = \int_{\mathcal{D}_{\mathbf{X}}} \mathcal{M}(\mathbf{X}) d\mathbf{X}, \quad (10)$$

and the others  $\mathcal{M}_i(X_i)$  and  $\mathcal{M}_{ij}(X_i, X_j)$  are the conditional mean values for parameters  $i$  and  $ij \mid i \neq j$ , respectively:

$$\mathcal{M}_i(X_i) = \int_0^1 \dots \int_0^1 \mathcal{M}(\mathbf{X}) d\mathbf{X}_{\sim i} - \mathcal{M}_0, \quad (11)$$

$$\mathcal{M}_{ij}(X_i, X_j) = \int_0^1 \cdots \int_0^1 \mathcal{M}(\mathbf{X}) d\mathbf{X}_{\sim ij} - \mathcal{M}_0 - \mathcal{M}_i(X_i) - \mathcal{M}_j(X_j). \quad (12)$$

The notation  $\sim i$  indicates that parameter  $X_i$  is excluded. Equation 9 has the property of orthogonality in terms of conditional means (HOMMA; SALTELLI, 1996), and it is possible to define the Sobol' decomposition in terms of conditional variances (SOBOL, 1993). Thus, one can compute the first-order Sobol' indices that quantify the additive effect of each input parameter separately concerning the total variance:

$$S_i = \frac{\text{Var}[\mathcal{M}_i(X_i)]}{\text{Var}[\mathcal{M}(\mathbf{X})]}, \quad (13)$$

and the second-order Sobol' indices that quantify the interaction effects between two input parameters:

$$S_{ij} = \frac{\text{Var}[\mathcal{M}_{ij}(X_i, X_j)]}{\text{Var}[\mathcal{M}(\mathbf{X})]}. \quad (14)$$

Higher-order Sobol' indices are equally defined and take into account the interaction effects of various input parameters.

## 2.2.2 Polynomial-Chaos expansion

Monte Carlo simulation can be used to compute Sobol' indices, although its high computational cost is due to the low convergence rate. An alternative way to calculate Sobol' indices is by constructing a surrogate model based on polynomial chaos expansion (PCE). Surrogate modeling consists of techniques that approximate a model in order to reduce computational cost while maintaining model accuracy. Sobol' indices are computed using PCE in (CRESTAUX; MAÎTRE; MARTINEZ, 2009; PALAR *et al.*, 2018).

PCE was developed by (WIENER, 1938). In engineering, PCE can be applied to the spectral analysis of stochastic finite elements (GHANEM, 2011). A non-intrusive method represents an uncertain quantity of interest through an expansion composed of deterministic coefficients and orthogonal polynomials. This paper is a review of global sensitivity analysis using PCE (SUDRET, 2008).

Based on PCE expression, the scalar output of interest  $Y$  can be rewritten as:

$$Y \approx \sum_{\alpha \in \mathcal{A}} y_\alpha \psi_\alpha(X). \quad (15)$$

In Equation 15,  $\psi_\alpha$  are multivariate polynomials that are orthonormal in relation to a joint probability density function  $f_{\mathbf{X}}$ ,  $y_\alpha$  are unknown deterministic coefficients and  $\mathcal{A}$  is a truncation criterion, where  $\mathcal{A} \subset \mathbb{N}^M$  is the set of selected multi-indices of multivari-

ate polynomials. The coefficients can be determined through the least angle regression method.

The statistics of an uncertain output response  $Y$  can be determined using PCE. Therefore, the mean and the variance are defined, respectively, by:

$$\mathcal{M}_0 = y_0 \quad \text{and} \quad \widehat{Var}[Y] = \sum_{\substack{\alpha \in \mathcal{A} \\ \alpha \neq 0}} y_\alpha^2. \quad (16)$$

Therefore, the PCE coefficients can directly determine the Sobol' indices with minor computational effort. Thus, the first and second-order Sobol' indices are, respectively:

$$S_i^{\text{PCE}} = \sum_{\substack{\alpha \in \mathcal{A}_i \\ \alpha \neq 0}} y_\alpha^2 / \sum_{\substack{\alpha \in \mathcal{A} \\ \alpha \neq 0}} y_\alpha^2, \quad (17)$$

$$S_{ij}^{\text{PCE}} = \sum_{\substack{\alpha \in \mathcal{A}_{ij} \\ \alpha \neq 0}} y_\alpha^2 / \sum_{\substack{\alpha \in \mathcal{A} \\ \alpha \neq 0}} y_\alpha^2. \quad (18)$$

In this work, a global sensitivity analysis is performed. The Sobol' indices are computed through the coefficients of a PCE-based surrogate model to verify the influence of the parameters of the Bouc-Wen model on the error measure.

## 2.3 THE CROSS-ENTROPY METHOD

The cross-entropy (CE) method translates an optimization problem into a rare event estimation problem, and this method can be treated as a two-step iterative process:

- First, random samples are generated according to a given probability distribution is determined feasible region;
- Then, the statistics, i.e., the mean and variance of a set composed of the best performing samples, are used to refine the probability distribution parameters.

Among other applications, the CE method can be used to solve continuous and combinatorial optimization problems (BOER *et al.*, 2005). Additional information about its theoretical framework and practical considerations about the optimization method can be found in (RUBINSTEIN; KROESE, 2011).

The central idea of the CE method is based on importance sampling technique and variance minimization. First, let  $X \sim f$  be a random variable with probability density

function (PDF)  $f$  and let  $H(X)$  be a function. The expected value of  $H(X)$  is:

$$\mu_f = \mathbb{E}_f\{H(X)\} = \int_{\mathcal{B}} H(x)f(x)dx. \quad (19)$$

Let  $g$  be other PDF. The expected value of  $H(X)\frac{f(X)}{g(X)}$  is:

$$\mu_g = \mathbb{E}_g\left\{H(X)\frac{f(X)}{g(X)}\right\} = \int_{\mathcal{B}} H(x)\frac{f(x)}{g(x)}g(x)dx, \quad (20)$$

and the importance sampling estimator  $\hat{\mu}_g$  is:

$$\hat{\mu}_g = \frac{1}{N_k} \sum_{k=0}^{N_k} H(x_k) \frac{f(x_k)}{g(x_k)}, \quad X \sim g, \quad (21)$$

where the term on the right defines  $W(x) = \frac{f(x)}{g(x)}$  the likelihood ratio. The quality of the estimator  $\hat{\mu}_g$  depends on the PDF  $g$ . The optimal importance sampling PDF  $\hat{g}^*$  is the one in which the variance of  $\hat{\mu}_g$  is minimal.

The Kullback-Leibler divergence denoted  $\mathcal{D}(g, h)$  offers a measure of how different a chosen PDF  $h$  is with respect to the reference PDF  $g$ . It is defined as follows in Equation 22:

$$\mathcal{D}(g, h) = \mathbb{E}_g\left\{\ln \frac{g(X)}{h(X)}\right\}. \quad (22)$$

The PDF  $f(\cdot; \mathbf{v})$  determined by the hyper-parameters vector  $\mathbf{v}$  is chosen. As it is shown in (KROESE; RUBINSTEIN; GLYNN, 2013), the minimization of  $\mathcal{D}(\hat{g}^*, f(\cdot, \mathbf{v}))$  leads to Equation 23, with  $\hat{g}^* \propto Hf(\cdot; \mathbf{u})$ :

$$\mathbf{v}^* = \arg \max_{\mathbf{w}} \mathbb{E}_{\mathbf{w}}\left\{H(x)W(x; \mathbf{u}, \mathbf{w}) \ln f(x; \mathbf{v})\right\} \quad (23)$$

Finally, for  $X_s \sim f(\cdot; \mathbf{w})$  and  $W(x_s; \mathbf{u}, \mathbf{w}) = \frac{f(\cdot; \mathbf{u})}{f(\cdot; \mathbf{w})}$ ,  $\hat{\mathbf{v}}$  is the hyper-parameter vector that approximates to the optimal importance estimator (minimal variance):

$$\hat{\mathbf{v}} = \arg \max_{\mathbf{w}} \frac{1}{N_k} \sum_{k=0}^{N_k} H(x_k)W(x_k; \mathbf{u}, \mathbf{w}) \ln f(x_k; \mathbf{v}). \quad (24)$$

Some assumptions are made in the sequence about the function  $H(x)$ . For rare event simulation and optimization problems,  $H(x) = \mathbb{1}_{J(x) \geq \epsilon}$  where  $\mathbb{1}_{J(x) \geq \epsilon}$  is the indicator



function and  $J(x)$  is an objective function. Specifically, in this work:

$$H(\boldsymbol{\theta}) = \mathbb{1}_{\bar{E}(\boldsymbol{\theta}) \geq \epsilon} = \begin{cases} 1 & \text{if } \bar{E}(\boldsymbol{\theta}) \geq \epsilon \\ 0 & \text{if } \bar{E}(\boldsymbol{\theta}) < \epsilon. \end{cases} \quad (25)$$

The expected value of the indicator function is the probability of the event  $\bar{E}(\boldsymbol{\theta}) \geq \epsilon$  to occur.

$$\mu = \mathbb{E}\{\mathbb{1}_{\bar{E}(\boldsymbol{\theta}) \geq \epsilon}\} = \mathcal{P}\{\bar{E}(\boldsymbol{\theta}) \geq \epsilon\}, \quad (26)$$

and its importance sampling estimator  $\hat{\mu}_g$  is:

$$\hat{\mu}_g = \frac{1}{N_k} \sum_{k=0}^{N_k} \mathbb{1}_{\bar{E}(\boldsymbol{\theta}^{(k)}) \geq \epsilon}. \quad (27)$$

(CUNHA, 2021) intuitively describes the computational algorithm of the CE method through the following steps:

1. **Initialize:** Choose initial hyper-parameters values  $\hat{\mu}_0$  and  $\hat{\sigma}_0^2$ , and  $\hat{\boldsymbol{v}}_0 = \{\hat{\mu}_0, \hat{\sigma}_0^2\}$ . Set level counter  $l = 1$ ;
2. **Sampling:** Generate  $N_k$  independent and identically distributed (iid) samples from the standard multivariate Gaussian distribution:

$$\boldsymbol{\theta}^{(1)}, \dots, \boldsymbol{\theta}^{(N_k)} \sim \mathcal{N}(\hat{\mu}_{l-1}, \hat{\sigma}_{l-1}^2);$$

3. **Select:** Evaluate the objective function for each sample and sort the  $N_k$  results in order:

$$\bar{E}(\boldsymbol{\theta}^{(\cdot)}) \leq \dots \leq \bar{E}(\boldsymbol{\theta}^{(\cdot)}).$$

The called elite sample set  $\mathcal{E}$  gathers the  $N_{\mathcal{E}} < N_k$  samples that better performed;

4. **Update:** Compute estimators:

$$\tilde{\mu}_l = \frac{1}{N_{\mathcal{E}}} \sum_{s=1}^{N_{\mathcal{E}}} \boldsymbol{\theta}^{(s)}, \quad (28)$$

$$\hat{\sigma}_l^2 = \frac{1}{N_{\mathcal{E}}} \sum_{s=1}^{N_{\mathcal{E}}} (\boldsymbol{\theta}^{(s)} - \tilde{\mu}_l)^2; \quad (29)$$

5. **Smooth:** Apply the smooth updating schema:

$$\hat{\mu}_l := a \cdot \tilde{\mu}_l + (1 - a) \cdot \hat{\mu}_{l-1}; \quad (30)$$

6. **Return**  $\hat{\boldsymbol{\theta}} = \hat{\mu}_l$  if the stopping criteria  $\hat{\sigma}_l^2 < \epsilon_{\max}$  is reached. Otherwise, increase level counter by 1 and return to the second step.

Operationally, the hyper-parameters vector  $\hat{\boldsymbol{v}}$  in Equation 24 can be estimated via maximum likelihood estimation method. The use of the standard multivariate Gaussian distribution (BOTTEV, 2016) on the sampling step of the CE method simplifies the estimation of  $\hat{\boldsymbol{v}}$  and the hyper-parameters can be computed directly by Equations 28 and 29.

Despite its mathematical formulation, the CE method can be easily implemented, and only few parameters that are pretty intuitive are needed: given the PDF  $f(\cdot; \boldsymbol{v})$ , the total number of samples  $N_s$ , the number of samples  $N_{\mathcal{E}}$  in the elite sample set, a stopping criterion  $\epsilon_{\max}$  and the maximum of iteration level  $l_{\max}$ .

To the sequence,  $\hat{E}$  can be computed using Equation 7 and the parameters of the Bouc-Wen model are considered as random quantities. Their distributions are inferred via Bayesian inference.

## 2.4 BAYESIAN INFERENCE

Bayesian inference approach is a straightforward strategy to quantify uncertainties (GELMAN *et al.*, 2013). A set of parameter is considered as a random input vector  $\boldsymbol{x}$  and the methodology to infer its distribution is based on the Bayes' theorem in Equation 31:

$$\pi(\boldsymbol{x}|\hat{\boldsymbol{E}}) = \frac{\pi(\hat{\boldsymbol{E}}|\boldsymbol{x})\pi(\boldsymbol{x})}{\pi(\hat{\boldsymbol{E}})}, \quad (31)$$

where  $\pi(\boldsymbol{x})$  is the prior distribution of the set of parameters  $\boldsymbol{x}$ ,  $\pi(\hat{\boldsymbol{E}}|\boldsymbol{x})$  is the likelihood function of  $\hat{\boldsymbol{E}}$  given a set of parameters  $\boldsymbol{x}$  at hand and  $\pi(\boldsymbol{x}|\hat{\boldsymbol{E}})$  is the posterior distribution of the set of parameters  $\boldsymbol{x}$  given  $\hat{\boldsymbol{E}}$ . The denominator  $\pi(\hat{\boldsymbol{E}})$  is the marginal likelihood: it is a normalized constant so the posterior distribution defines a probability density function with integral equal to the unity. In this case, Equation 31 can be simplified into:

$$\pi(\boldsymbol{x}|\hat{\boldsymbol{E}}) \propto \pi(\hat{\boldsymbol{E}}|\boldsymbol{x})\pi(\boldsymbol{x}). \quad (32)$$

The prior distribution  $\pi(\boldsymbol{x})$  can be interpreted as the knowledge degree about  $\boldsymbol{x}$  before any evidence. It is classified based on its influence on the posterior distribution, and an example of a diffuse – or non-informative – prior is a Uniform prior distribution. In this case, Equation 32 can also be simplified into:

$$\pi(\boldsymbol{x}|\hat{\boldsymbol{E}}) \propto \pi(\hat{\boldsymbol{E}}|\boldsymbol{x}). \quad (33)$$

One assumes that  $\hat{E}$  is the error measure  $\bar{E}(\boldsymbol{\theta})$  from the suggested model plus a

discrepancy term  $\epsilon$  that is the source of uncertainty:

$$\hat{E} = \bar{E}(\boldsymbol{\theta}) + \epsilon, \quad (34)$$

and it is supposed an additive Gaussian discrepancy with mean  $\mu_\epsilon = 0$  and unknown variance  $\sigma_\epsilon^2$ . One can demonstrate that in cases where  $\mu_\epsilon = 0$  and  $\sigma_\epsilon^2$  is known, the additive Gaussian discrepancy model corresponds to the MaxEnt<sup>3</sup> principle (SOIZE, 2017). In this case,  $\epsilon \sim \mathcal{N}(0, \sigma_\epsilon^2)$  and:

$$\pi(\hat{E} | \boldsymbol{x} = \{\boldsymbol{\theta}, \sigma_\epsilon^2\}) \sim \mathcal{N}(\hat{E} | \bar{E}(\boldsymbol{\theta}), \sigma_\epsilon^2). \quad (35)$$

In the case of independent and identically distributed (iid) observations, the likelihood function is defined as:

$$\pi(\hat{\boldsymbol{E}} | \boldsymbol{x}) = \prod_{i=1}^N \pi(\hat{E}_i | \boldsymbol{x}) = \frac{1}{\sqrt{2\pi\sigma_\epsilon^2}} \exp\left(-\frac{1}{2} \sum_{i=1}^N \frac{(\hat{E}_i - \bar{E}(\boldsymbol{\theta}))^2}{\sigma_\epsilon^2}\right), \quad (36)$$

and after Equations 33 and 36, the posterior distribution can be finally defined as follows:

$$\pi(\boldsymbol{x} | \hat{\boldsymbol{E}}) \propto \frac{1}{\sqrt{\sigma_\epsilon^2}} \exp\left(-\frac{1}{2} \sum_{i=1}^N \frac{(\hat{E}_i - \bar{E}(\boldsymbol{\theta}))^2}{\sigma_\epsilon^2}\right). \quad (37)$$

### 2.4.1 Markov chain Monte Carlo

To determine the posterior distribution  $\pi(\boldsymbol{x} | \hat{\boldsymbol{E}})$  of parameters  $\boldsymbol{x}$  given  $\hat{\boldsymbol{E}}$  is not always trivial. Usually, Monte Carlo simulation is used to approximate the solutions. This book is a review on Monte Carlo methods (KROESE; TAIMRE; BOTEV, 2011).

The Metropolis-Hastings algorithm is a Markov chain Monte Carlo (MCMC) method based on the construction of a Markov chain such that the future state  $\boldsymbol{x}^{(k+1)}$  of the chain depends only on its current state  $\boldsymbol{x}^{(k)}$  and a transition probability distribution  $\mathcal{T}(\boldsymbol{x}^{(k+1)} | \boldsymbol{x}^{(k)})$ . In the presence of a sufficient number of unbiased samples, the sequence of random variables  $\boldsymbol{X} = \{\boldsymbol{x}^{(0)}, \boldsymbol{x}^{(1)}, \boldsymbol{x}^{(2)}, \dots\}$  represents the posterior distribution  $\pi(\boldsymbol{x} | \hat{\boldsymbol{E}})$ :

$$\frac{\pi(\boldsymbol{x}^{(k+1)} | \hat{\boldsymbol{E}})}{\pi(\boldsymbol{x}^{(k)} | \hat{\boldsymbol{E}})} = \frac{\mathcal{T}(\boldsymbol{x}^{(k+1)} | \boldsymbol{x}^{(k)})}{\mathcal{T}(\boldsymbol{x}^{(k)} | \boldsymbol{x}^{(k+1)})}. \quad (38)$$

The procedure for generating the future state  $\boldsymbol{x}^{(k+1)}$  is a two-stage process: the first stage is to generate a candidate  $\boldsymbol{x}^{(*)}$  that depends only on the current state  $\boldsymbol{x}^{(k)}$  of the Markov chain; the second stage is to accept or reject  $\boldsymbol{x}^{(*)}$ . To this end, it is necessary

<sup>3</sup>The MaxEnt principle establishes the distribution that maximizes the entropy, depending on the available information (mean, variance, support, etc.) about a system.

to compute the acceptance probability  $a$  according to Equation 39, where  $\mathcal{K}(\mathbf{x}^{(*)}|\mathbf{x}^{(k)})$  is the proposed probability distribution:

$$a = \min \left\{ 1, \frac{\pi(\mathbf{x}^{(*)}|\hat{\mathbf{E}}) \mathcal{K}(\mathbf{x}^{(*)}|\mathbf{x}^{(k)})}{\pi(\mathbf{x}^{(k)}|\hat{\mathbf{E}}) \mathcal{K}(\mathbf{x}^{(k)}|\mathbf{x}^{(*)})} \right\}. \quad (39)$$

Then, a random number  $u \sim \mathcal{U}(0, 1)$  is generated from a Uniform distribution with parameters 0 and 1. If  $u < a$ , the candidate  $\mathbf{x}^{(*)}$  is accepted and  $\mathbf{x}^{(k+1)} = \mathbf{x}^{(*)}$ . Otherwise, if  $u \geq a$ ,  $\mathbf{x}^{(*)}$  is rejected and  $\mathbf{x}^{(k+1)} = \mathbf{x}^{(k)}$ .

The random walk Metropolis algorithm is a particular case of the Metropolis-Hastings algorithm. In it, a symmetric Gaussian distribution with variance  $\sigma^2$  is proposed to generate the candidate  $\mathbf{x}^{(*)}$  (SAADI; YKHLEF; GUESSOUM, 2011) yielding:

$$a = \min \left\{ 1, \frac{\pi(\mathbf{x}^{(*)}|\hat{\mathbf{E}})}{\pi(\mathbf{x}^{(k)}|\hat{\mathbf{E}})} \right\}. \quad (40)$$

The following steps summarizes the random walk Metropolis algorithm:

1. Initialize the counter and assign initial value  $\mathbf{x}^{(0)}$ ;
2. Generate a candidate  $\mathbf{x}^{(*)} \sim \mathcal{N}(\mathbf{x}^{(k)}, \sigma^2)$ ;
3. Compute the acceptance probability  $a(\mathbf{x}^{(*)}, \mathbf{x}^{(k)})$  and generate a random number  $u \sim \mathcal{U}(0, 1)$ ;
4. Does  $u < a$ ? If positive, accept the candidate and  $\mathbf{x}^{(k+1)} = \mathbf{x}^{(*)}$ . If negative, reject and  $\mathbf{x}^{(k+1)} = \mathbf{x}^{(k)}$ ;
5. Increment the counter and return to the second step.

This article adopted some strategies while implementing the Metropolis-Hastings algorithm to accelerate the convergence of the Markov chain (SAADI; YKHLEF; GUESSOUM, 2011). A first feature is the total number of generated samples: the Markov chain must be large enough to adequately represent the distributions of the parameters respecting the law of large numbers. The second one is the acceptance probability rate  $\bar{a} = \frac{N_a}{N_k}$  that is the ratio between the number of accepted samples  $N_a$  and the total number of generated samples  $N_k$ .  $\bar{a}$  is controlled by the random walk step  $\sigma$ : on the one hand, if the jump from one sample to the other is too large,  $\bar{a}$  is small, and the chain keeps static; on the other hand, if the jump from one sample to the other is too small,  $\bar{a}$  is big, and the chain needs more time to go through the parameters space. One considers the optimal  $\bar{a}$  between 40% – 50% (SAADI; YKHLEF; GUESSOUM, 2011). The last feature is the burn-in: eliminat-

ing a defined number of initials samples from the final result. This feature is essential to eliminate biased results.

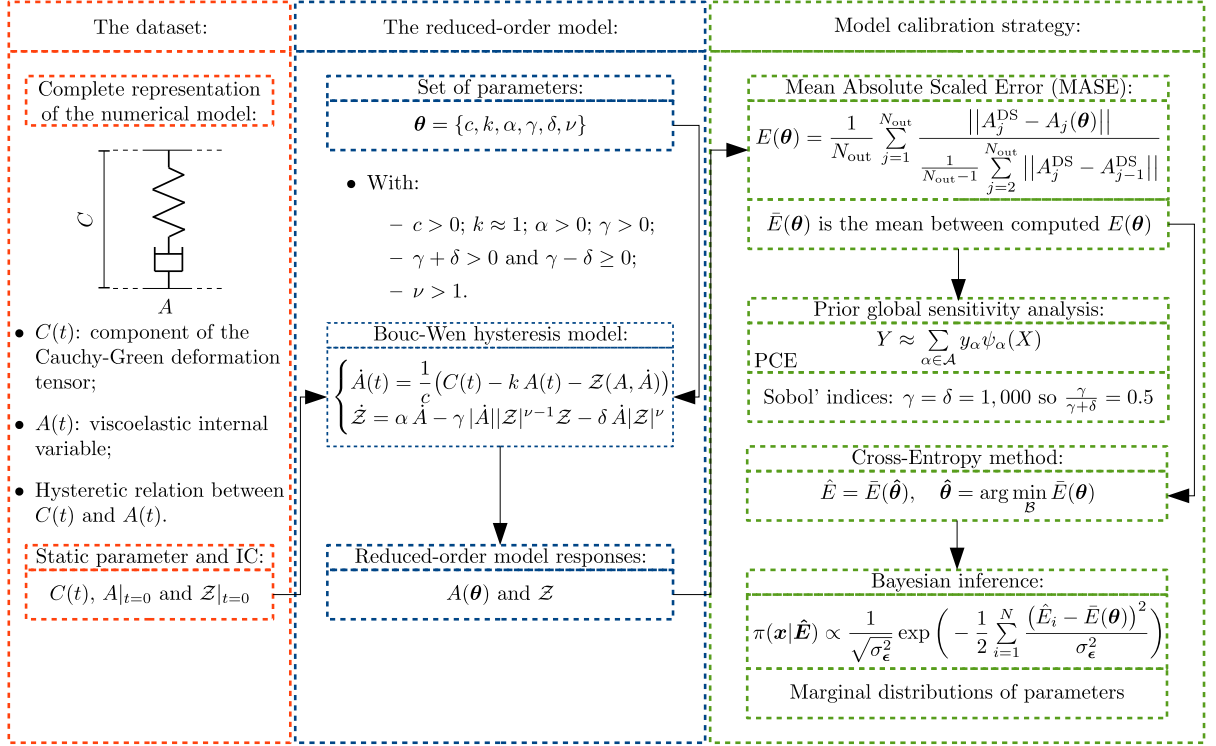
## 2.5 CONCLUDING REMARKS

This chapter's central importance is registering the theoretical background of the adopted calibration strategy. At the beginning, an error metric is defined to quantify the differences between the responses of the formulated model and the data. Adopting a practical point of view, the prior global sensitivity analysis aims to determine which parameters of the Bouc-Wen model influence the variability of the error metric. The parameters whose Sobol' indices are negligible can be considered as constant quantities to save processing time during the model calibration. The Cross-Entropy method aims to compute the optimal set of parameters from which the error metric is minimal. In addition, the optimal parameters provide complementary information for determining the prior distributions of the Bayesian inference. This latter aims to determine the distributions of the parameters through the posterior distribution of parameters given the data of viscoelastic internal variables. These distributions can propagate the uncertainties in the error metric and the suggested model responses. The construction of a model that takes into account the uncertainties in its formulation can contribute to the development of more robust tires. Figure 7 is a schematic that describes the steps in this work, including the model calibration strategy:

Instead of applying complex techniques to construct and then calibrate the Bouc-Wen model, the insights of this methodology are:

1. Even treating a complex nonlinear problem such as viscoelasticity, the suggested model consists of a simple system of nonlinear differential equations. This system can be solved numerically with reduced computational cost;
2. Sobol' indices evaluate the importance of the parameters, in combination or individually, on the variability of the responses and justify the necessity to calibrate or not a parameter. In this way, this methodology determines which parameters should be calibrated. In addition, Sobol' indices can be evaluated with little computational costs from the coefficients of a PCE-surrogate model;
3. The cross-entropy method guarantees convergence;
4. Both the cross-entropy method and the Bayesian inference can be easily implemented. In addition, Sobol' indices can be evaluated using open-sources libraries such as UQLab (MARELLI; SUDRET, 2014);

Figure 7: A schematic of the different steps in this work, including the model calibration strategy.



Source: Author's own elaboration.

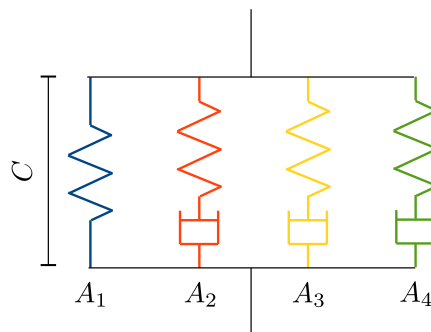
5. The suggested model is calibrated using data that originated from a finite element model, the standard model in the tire industry;
6. The same approach could be used to solve other structural dynamics problems, e.g., friction models with a population of sliders such as the Iwan model (SEGALMAN, 2005)).

### 3 RESULTS AND DISCUSSION

By adopting the model calibration strategy from Chapter 2, this chapter calibrates a set of Bouc-Wen models and presents results that justify that the methods that compose the model calibration strategy were adequately used: initially, a preliminary global sensitivity analysis is conducted by evaluating the Sobol' indices from the coefficients of a PCE-based surrogate model; next, the minimum error metric is computed using the Cross-Entropy Method. The model parameters that give the minimum error metric are considered optimal; then, Bayesian inference is used to determine the distributions of the influential parameters of the suggested model.

As stated in Chapter 1, the complete model is formed by the first 4 Maxwell branches of the generalised Maxwell model. In these branches, the viscoelastic internal variables present dynamic behavior. Figure 8 recalls the complete model:

Figure 8: A recall of the complete model. Branches of interest: Branches 1, 2, 3 and 4.



Source: Author's own elaboration.

Through numerical simulations, it was observed that better results were archived when the inputs were divided into 2 groups: Group 1 and 2. Thus, the total work to be done consists of calibrating 8 models (Branches 1, 2, 3 and 4  $\times$  Group 1 and 2). As the same model calibration strategy was applied to them, to avoid repetition, the results related to the calibration procedure are presented to Branch 1, Group 1 only. Otherwise, the results associated with determining the distributions of error metrics are presented to the 8 models.

---

### 3.1 BOUC-WEN MODEL CALIBRATION

The MATLAB scripts used in numerical simulations are available in the following GitHub repository: [https://github.com/rafaelraqueti/UQ\\_Bouc-Wen\\_calibration.git](https://github.com/rafaelraqueti/UQ_Bouc-Wen_calibration.git). As the dataset belongs to Michelin, it is unavailable in this repository.

It is assumed that the parameters of a Bouc-Wen model follow a Uniform distribution  $\mathcal{U}(a, b)$  with support  $a$  and  $b$ , which are respectively the minimum and maximum values. This assumption was made because any event in a Uniform distribution is equally likely to be chosen. Table 1 shows the minimum and maximum values used in the prior global sensitivity analysis. The bounds  $a$  and  $b$  were chosen respecting the physical and mathematical consistency of the Bouc-Wen model.

Table 1: Uniform distributions of the parameters of the Bouc-Wen model used in the prior global sensitivity analysis.

$\mathcal{U}(a, b)$	$c$	$k$	$\alpha$	$\gamma$	$\delta$	$\nu$
$a$	0	0.999	0	1,000	-1,000	1
$b$	0.01	1.001	1	10,000	1,000	3

Source: Author’s own elaboration.

The prior global sensitivity analysis was performed to verify which parameters of the proposed model are influential. To do so, a PCE-based surrogate model  $\tilde{E}(\boldsymbol{\theta})$  was built as an alternative to evaluate the error metric  $\bar{E}(\boldsymbol{\theta})$ . The coefficients of the PCE-based surrogate model were computed using the UQLab metamodeling module (MARELLI; LÜTHEN; SUDRET, 2022). Table 2 contains information about the PCE-based surrogate model: the PCE degree was selected by the UQLab module by verifying which surrogate model with the PCE degree between 1 and 15 performed the best.

Table 2: Information about the PCE-based surrogate model.

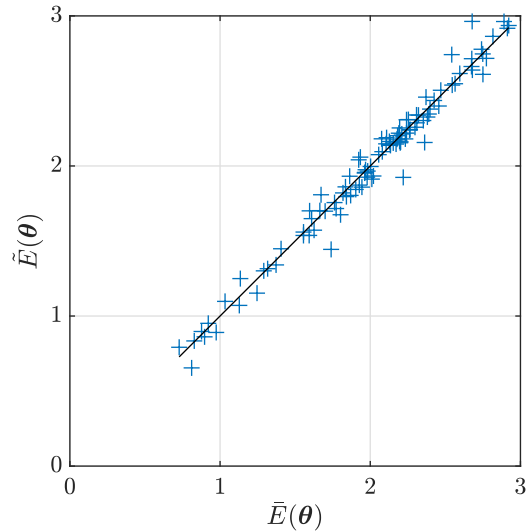
PCE degree	qNorm	Exp. Design	LOO error	Time [min]
13	0.75	1,000	$1.7 \cdot 10^{-2}$	25

Source: Author’s own elaboration.

Figure 9 compares the error metrics  $\bar{E}(\boldsymbol{\theta})$  and  $\tilde{E}(\boldsymbol{\theta})$ : the closer to the black diagonal line, the more reliable the PCE-based surrogate model is. In Figure 9, both  $\bar{E}(\boldsymbol{\theta})$  and  $\tilde{E}(\boldsymbol{\theta})$  were evaluated using 100 cross-validation samples, i.e., samples that were not used to build the PCE-based surrogate model. It is worth mentioning that the model is not yet calibrated. That is why it is normal to observe in Figure 9 values of the error measure higher than the unity.



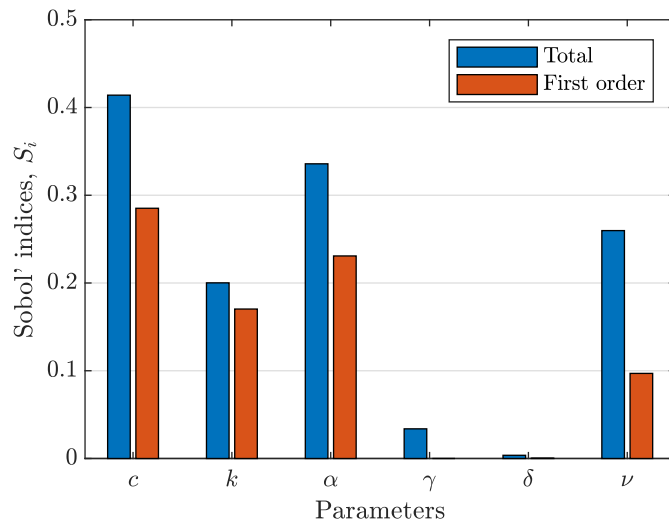
Figure 9: Branch 1, Group 1 – Comparison between error metrics  $\bar{E}(\boldsymbol{\theta})$  and  $\tilde{E}(\boldsymbol{\theta})$ . The disposition of the 100 cross-validation samples  $+$  indicates that the PCE-based surrogate model is adequate.



Source: Author's own elaboration.

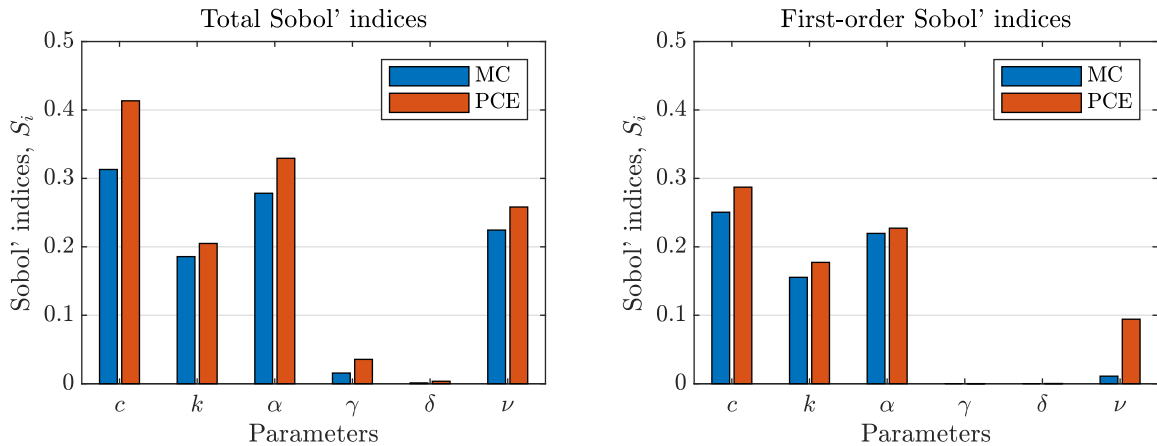
Once the PCE-based surrogate model was built and validated, the Sobol' indices were computed from its coefficients with minor computational effort using the UQLab sensitivity analysis module (MARELLI *et al.*, 2022). This global sensitivity analysis allows conclusions about the Bouc-Wen model parameters before inferring their distributions. Figure 10 shows the total and first-order Sobol' indices. These values are compared with the Sobol' indices computed using Monte Carlo simulation in Figure 11 (a maximum of 100 model evaluations). The Sobol' indices based on PCE were considered adequate.

Figure 10: Branch 1, Group 1 – Prior global sensitivity analysis. Total and first-order Sobol' indices of parameters  $\gamma$  and  $\delta$  are negligible. Therefore,  $\gamma$  and  $\delta$  can be considered as completely determined quantities.



Source: Author's own elaboration.

Figure 11: Comparison between Sobol' indices based on Monte Carlo estimation and polynomial chaos expansion.



Source: Author's own elaboration.

On the one side, the total and first-order Sobol' indices of parameters  $\gamma$  and  $\delta$  indicate little influence on the error metric. In this sense, having less or more variability on these parameters does not mean that the suggested model simulates viscoelastic internal variables more accurately. For this reason, they were considered as completely determined quantities and their values were set to  $\gamma = 1000$  and  $\delta = 1000$  so  $\frac{\gamma}{\gamma+\delta} = 0.5$ , a limit condition for uniqueness of the solution (ISMAIL; IKHOUANE; RODELLAR, 2009). However, the total Sobol' index of parameter  $\gamma$  is not negligible. This indicates that the parameter  $\gamma$  can influence the error metric when combined with other parameters. On the other side, parameters  $c$ ,  $\alpha$ ,  $k$ , and  $\nu$  have considerable influence, and their variability requires attention, so they were considered unknowns. It is worth mentioning that total, and first-order Sobol' indices of parameters  $c$ ,  $k$  and  $\alpha$  are close (for  $k$  it is the more evident). This indicates that the higher-order indices are relatively small, and the influences of these parameters, when combined, are less significant than the individual influences. The same conclusions were assumed for the other models.

After the prior global sensitivity analysis, the error metric was considered as an optimization problem and the solution of Equation 7 was computed using the CE method. The parameters of the CE method of this step were:  $N_s = 100$  samples,  $N_\varepsilon = 4$  samples,  $l_{\max} = 500$  iterations and  $\epsilon_{\max} = 10^{-6}$ . A smooth updating schema of  $a = 0.8$  was also used. The same configuration was adopted to the other models. Table 3 shows the elapsed time to estimate the optimal parameters values:

After solving the optimization problem through the CE method,  $\hat{E} = 0.3171$  for Branch 1, Group 1, which is less than the values in Figure 9. The optimal values in Table 3 can be used to simulate viscoelastic internal variables. However, it is desirable to verify how the uncertainties propagate in the response of the suggested model. For this, the parameters  $c$ ,  $k$ ,  $\alpha$ ,  $\nu$  and the variance of the discrepancy  $\sigma_\varepsilon^2$  were calibrated using

Table 3: Branch 1 – Cross-Entropy method. Elapsed time and optimal values of the influential parameters of the Bouc-Wen model.

Group	$\hat{c}$	$\hat{k}$	$\hat{\alpha}$	$\hat{\nu}$	$\hat{E}$	Time [min]
Group 1	0.0018	1.0000	0.1152	1.0220	0.3171	63
Group 2	0.0035	1.0000	0.0418	1.8039	0.3655	39

Source: Author's own elaboration.

Bayesian inference according to the following procedure:

1. The bounds  $a$  and  $b$  of the Uniform prior distribution  $\mathcal{U}(a, b)$  are redefined according to Tables 4 and 5, depending on the branch of interest;
2. Initially, a Markov chain containing a total of  $N_k = 10^3$  samples were generated. The random walk step size  $\sigma$  was manually adjusted, and this step was repeated until the acceptance rate was  $\bar{a} \approx 40 - 50\%$ ;
3. Then, a Markov chain containing  $N_k = 10^5$  samples was generated. In this condition,  $\bar{a}$  did not change its value significantly. These samples were used to study the convergence of the Markov chain;
4. Finally, 2 other Markov chains containing a reduced number of samples were generated to verify the chain stability.

Table 4: Branches 1, 2 and 3 – Bayesian inference. Uniform prior distribution of the parameters of the Bouc-Wen model and the variance of the discrepancy.

$\mathcal{U}(a, b)$	$c$	$k$	$\alpha$	$\nu$	$\sigma_\epsilon^2$
$a$	0	0.999	0	1	0
$b$	0.01	1.001	1	3	0.1

Source: Author's own elaboration.

Table 5: Branch 4 – Bayesian inference. Uniform prior distribution of the parameters of the Bouc-Wen model and the variance of the discrepancy.

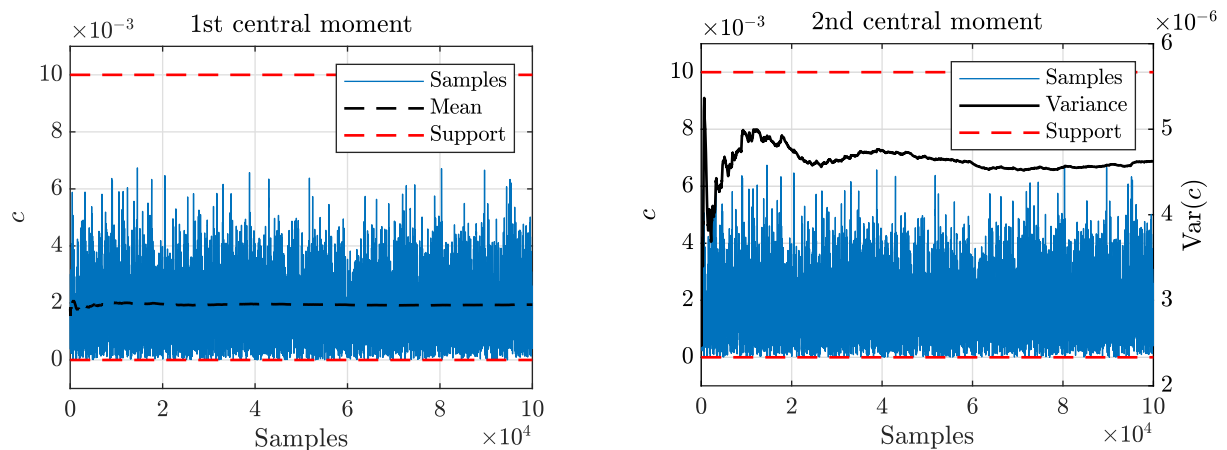
$\mathcal{U}(a, b)$	$c$	$k$	$\alpha$	$\nu$	$\sigma_\epsilon^2$
$a$	0	0.999	0	1	0
$b$	0.03	1.001	2	3	0.1

Source: Author's own elaboration.

To illustrate this procedure, Figure 12 to 16 show, for Branch 1, Group 1: 1) the trace plot of the proposed model parameters  $c$ ,  $k$ ,  $\alpha$  and  $\nu$ ; 2) the trace plot of the variance of the discrepancy  $\sigma_\epsilon^2$ ; 3) at the left, the convergence study of the first central moment

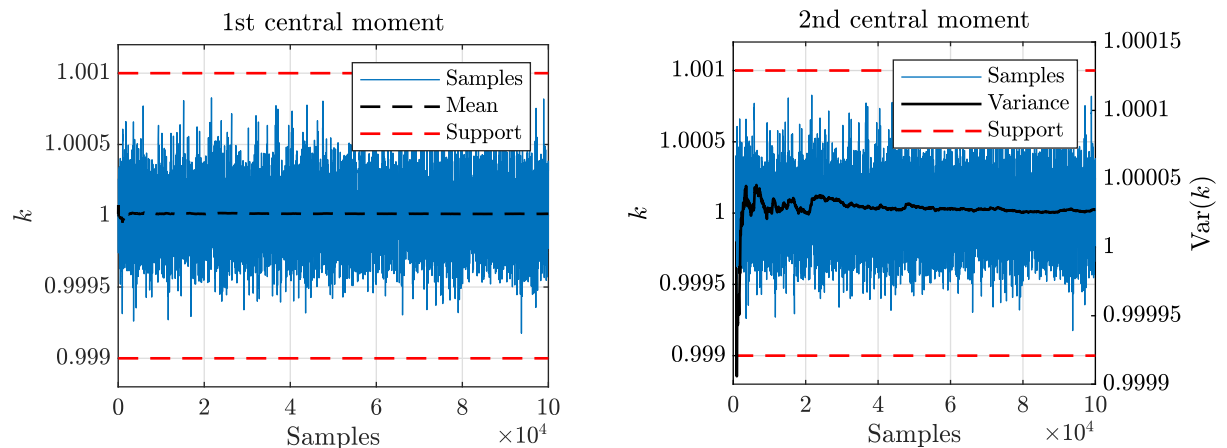
(mean); 4) at the right, the convergence study of the second central moment (variance). For these and the next figures, "Samples" in the legend refer to the samples that compose a Markov chain. Visually, both first and second central moments converged considering  $N_k = 10^5$  samples. Furthermore, Figure 15 indicates the minimum number of  $N_k = 2 \times 10^4$  samples for which the first and second central moments converged.

Figure 12: Branch 1, Group 1 – Bayesian inference. Convergence study of parameter  $c$ : first (Mean) and second central moments (Variance). The acceptance rate is  $\bar{a} \approx 43\%$  and no burn-in samples were considered.



Source: Author's own elaboration.

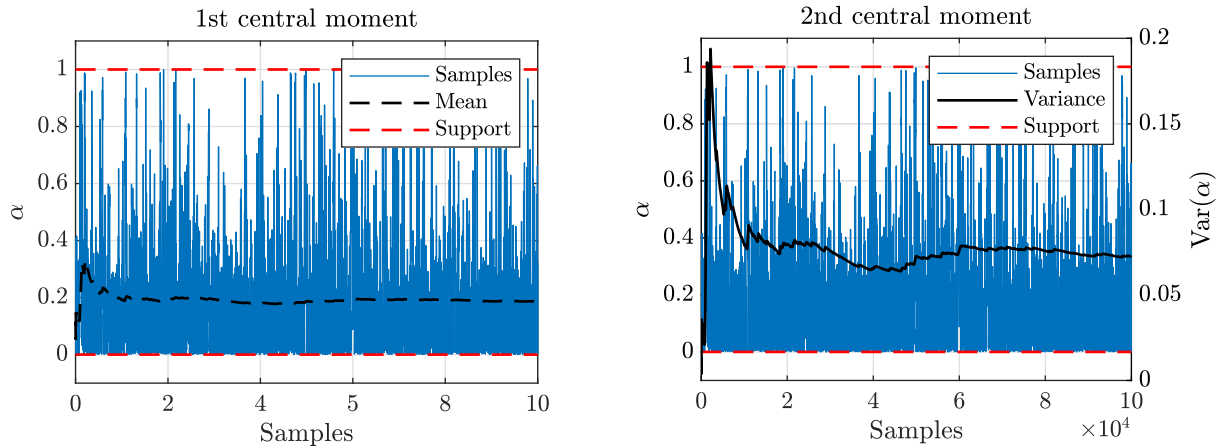
Figure 13: Branch 1, Group 1 – Bayesian inference. Convergence study of parameter  $k$ : first (Mean) and second central moments (Variance). The acceptance rate is  $\bar{a} \approx 43\%$  and no burn-in samples were considered.



Source: Author's own elaboration.

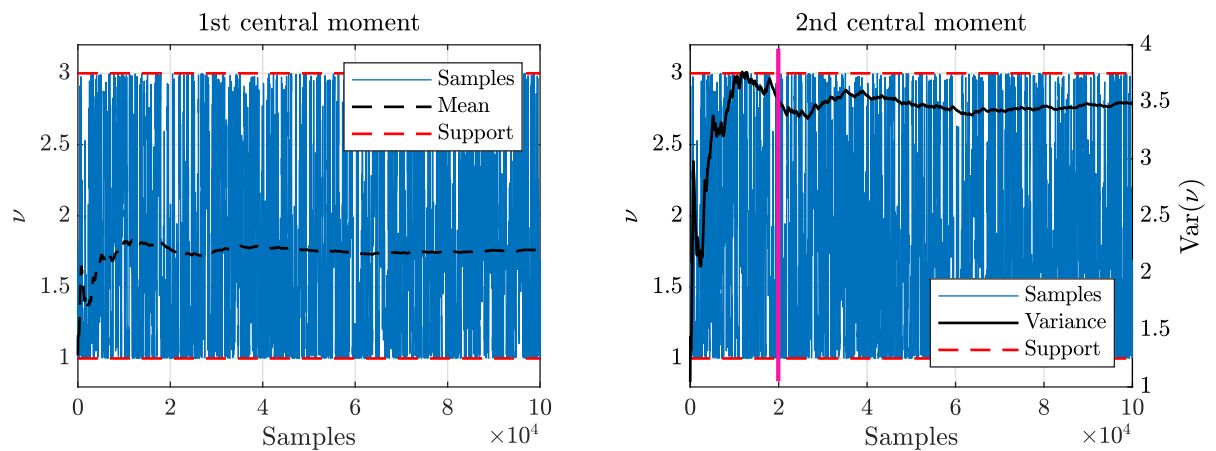
Then, two other Markov chains containing the minimum number of  $N_k = 2 \times 10^4$  samples were generated using different random number generator seeds. In Figure 17, the 3 Markov chains are equally distributed in the space defined by support  $a$  and  $b$ . In addition, there was no need to eliminate burn-in samples.

Figure 14: Branch 1, Group 1 – Bayesian inference. Convergence study of parameter  $\alpha$ : first (Mean) and second central moments (Variance). The acceptance rate is  $\bar{a} \approx 43\%$  and no burn-in samples were considered.



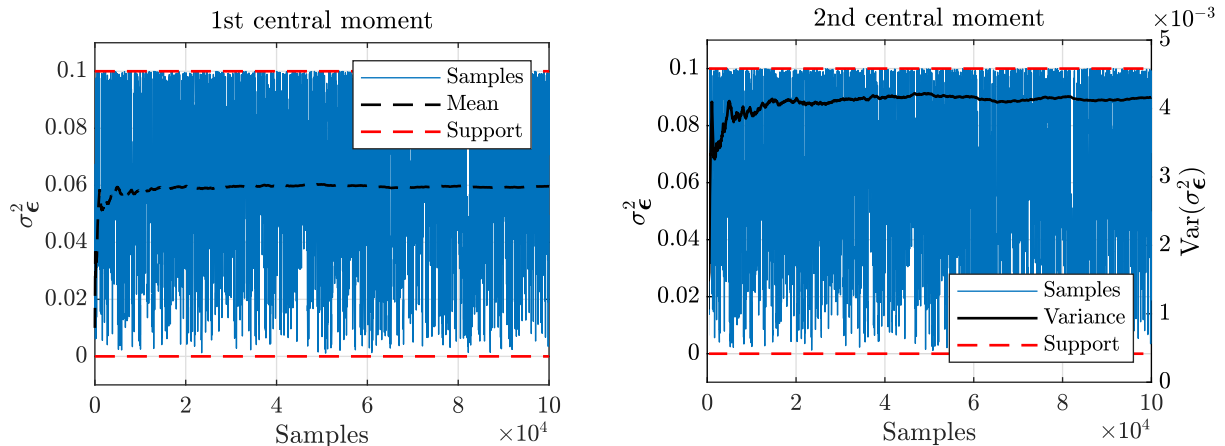
Source: Author's own elaboration.

Figure 15: Branch 1, Group 1 – Bayesian inference. Convergence study of parameter  $\nu$ : first (Mean) and second central moments (Variance). The acceptance rate is  $\bar{a} \approx 43\%$  and no burn-in samples were considered. Number of samples to reach convergence is  $2 \times 10^4$  samples (indicated by the magenta vertical line).



Source: Author's own elaboration.

Figure 16: Branch 1, Group 1 – Bayesian inference. Convergence study of the variance of the discrepancy: first (Mean) and second central moments (Variance). The acceptance rate is  $\bar{a} \approx 43\%$  and no burn-in samples were considered.



Source: Author's own elaboration.

The adopted procedure in the Bayesian inference step is essential because it guarantees the convergence and stability of the Markov chain. In addition, it allows them to establish a pattern to calibrate the other models. Because the Monte Carlo simulation is the most computationally expensive step from the model calibration strategy, determining the minimum number of samples and excluding burn-in samples reduces computational effort. The Markov chains were then used to estimate the distributions of the influential parameters of the Bouc-Wen model. The elapsed time to evaluate the values of the significant parameters is indicated in Table 6.

Table 6: Branch 1, Group 1 - Bayesian inference. Elapsed time to estimate the values of the parameters of the Bouc-Wen model and the variance of the discrepancy.  $N_k = 2 \times 10^4$  samples.

Branch	Group	$\sigma^2$	$\bar{a}$ [%]	Time [min]
Branch 1	Group 1	0.09	43	311
	Group 2	0.07	43	172

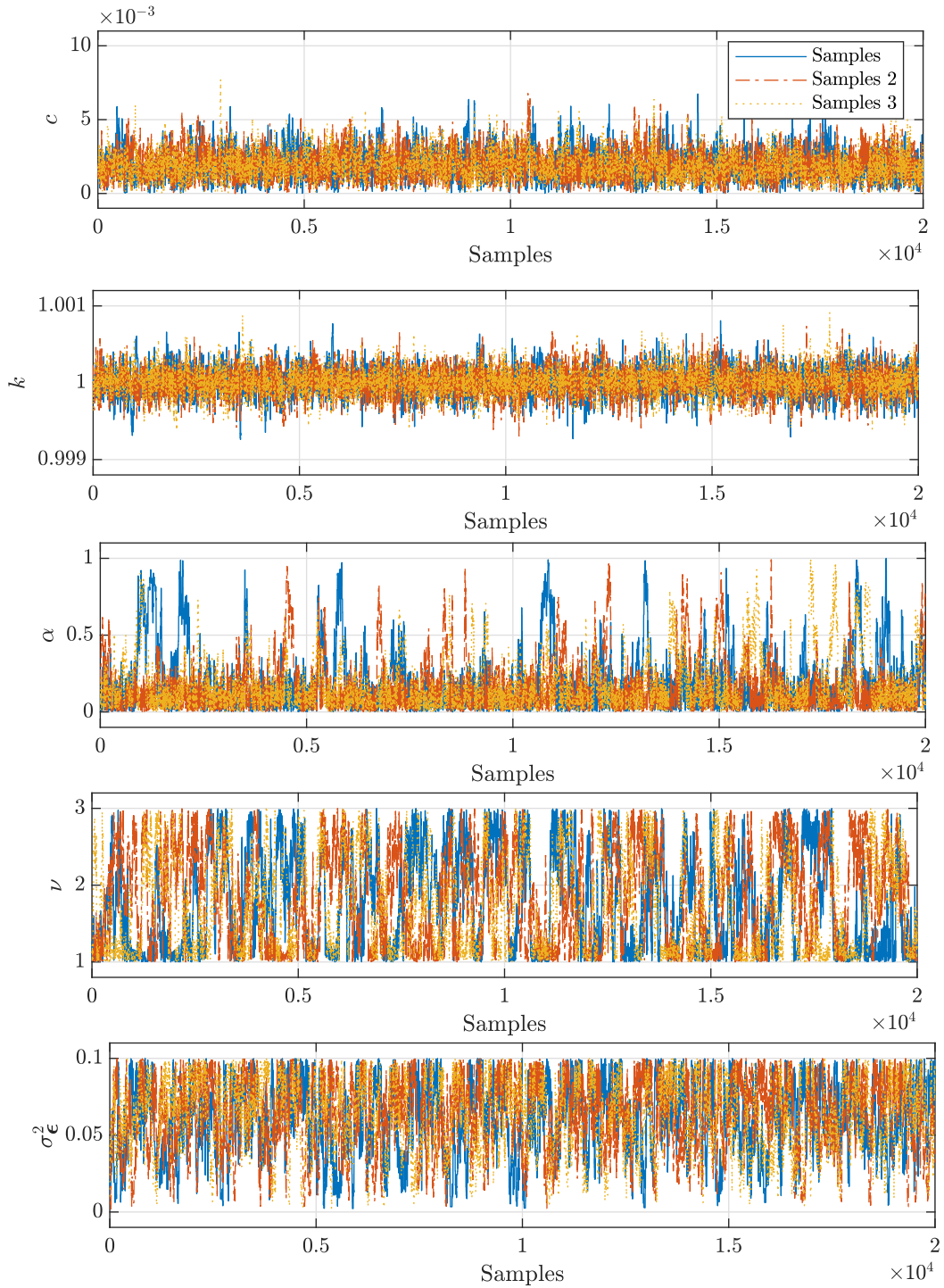
Source: Author's own elaboration.

Figure 18 shows the densities and cumulative densities of each one of the calibrated parameters, where the continuous black line is the probability density estimates (EPDF) based on a normal kernel function, the black dashed line is the Uniform prior distribution, and the marked red line is the empirical cumulative distribution function (ECDF).

From these distributions:

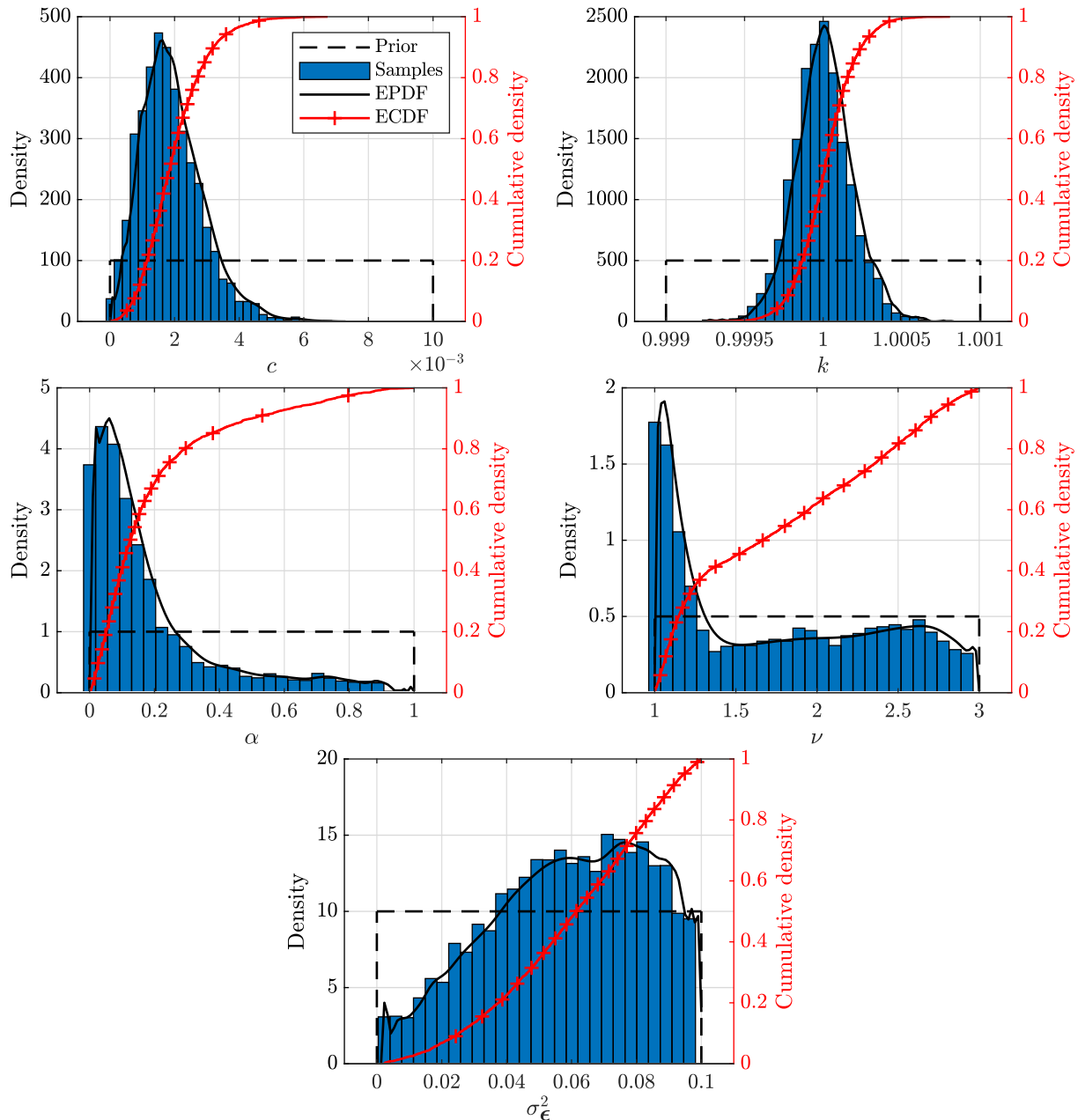
- It is possible to notice that the samples are centered around 0.002 and 1 for parameters  $c$  and  $k$ , respectively. There is a good agreement between the mean of their

Figure 17: Branch 1, Group 1 – Bayesian inference. Trace plots of the parameters of the Bouc-Wen model and the variance of the discrepancy: the samples were generated using different random number generator seeds.



Source: Author's own elaboration.

Figure 18: Branch 1, Group 1 – Bayesian inference. Distributions of the parameters of the Bouc-Wen model and variance of the discrepancy: Uniform prior (Prior), estimated probability density functions (EPDF) and empirical cumulative distribution functions (ECDF).



Source: Author's own elaboration.

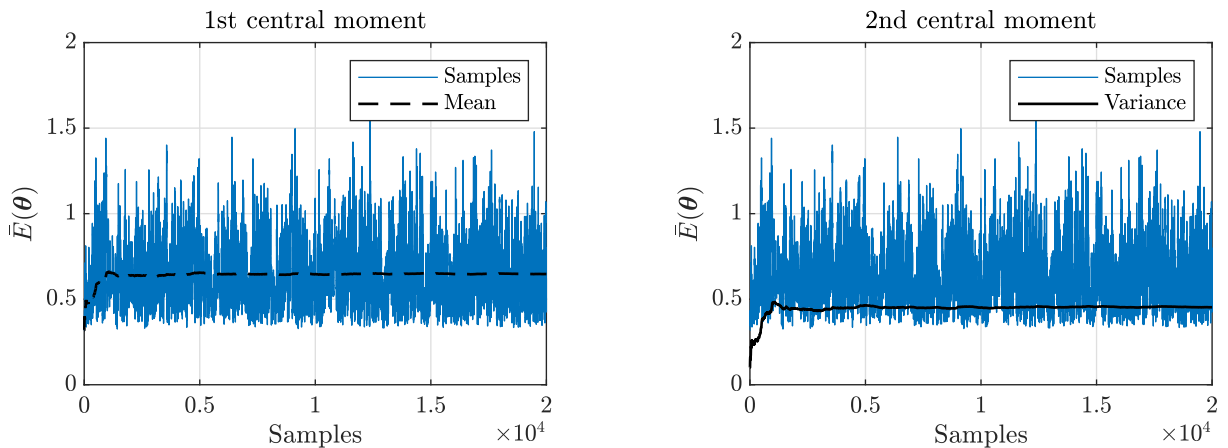


distributions and the optimal value computed through the Cross-Entropy method in Table 3;

- There is a higher tendency for parameter  $\alpha$  to get values between 0 and 0.2. Equally, there is a higher tendency for parameter  $\nu$  to get values close to 1. There is also a good agreement between their mean and the optimal value in Table 3.

Similarly, the same convergence study was done for the error metric of Branch 1, Group 1. The error metric is defined in Equation 6. Figure 19 shows that both the mean and variance converged considering the optimal number of samples. Figures 20 to 23 show the density and cumulative density function of the error metrics of all branches of interest. In these figures, the continuous black line is the probability density estimates (EPDF) based on a normal kernel function, and the marked red line is the empirical cumulative distribution function (ECDF). The vertical dashed magenta line indicates the optimal value  $\hat{E}$  of the error metric determined by the CE method. It is worth mentioning that  $\hat{E}$  has low probability of occurrence. On the one hand, from their ECDF, there is a high probability of having  $E(\theta) \leq 1$  in Branches from 1 to 3. On the other hand, Branch 4 optimal value  $\hat{E}$  of the error metric is already higher than 1. By adopting this criterion, this specific model is not suitable for simulating viscoelastic internal variables from Branch 4.

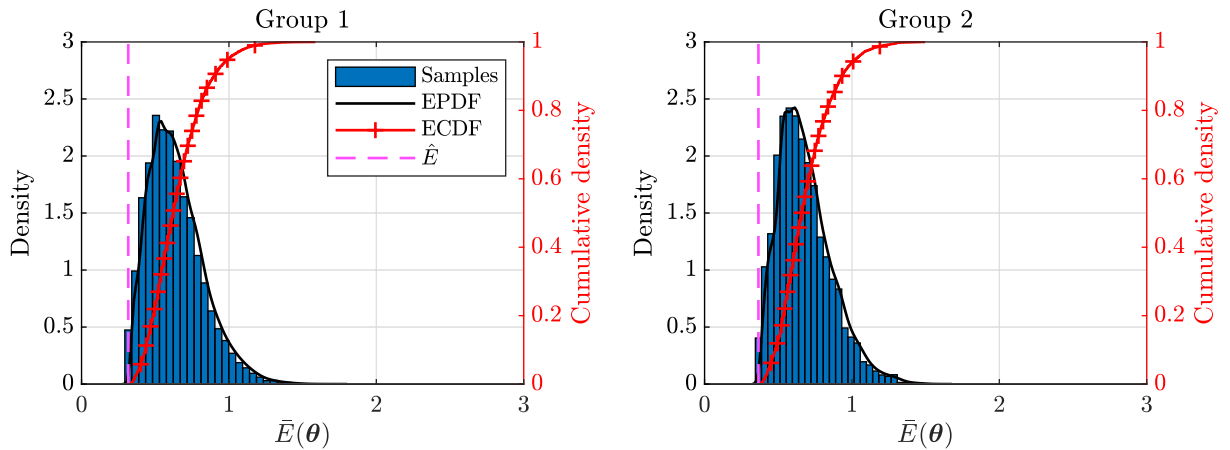
Figure 19: Branch 1, Group 1 - Convergence study of the error metric: first (Mean) and second central moments (Variance).



Source: Author's own elaboration.

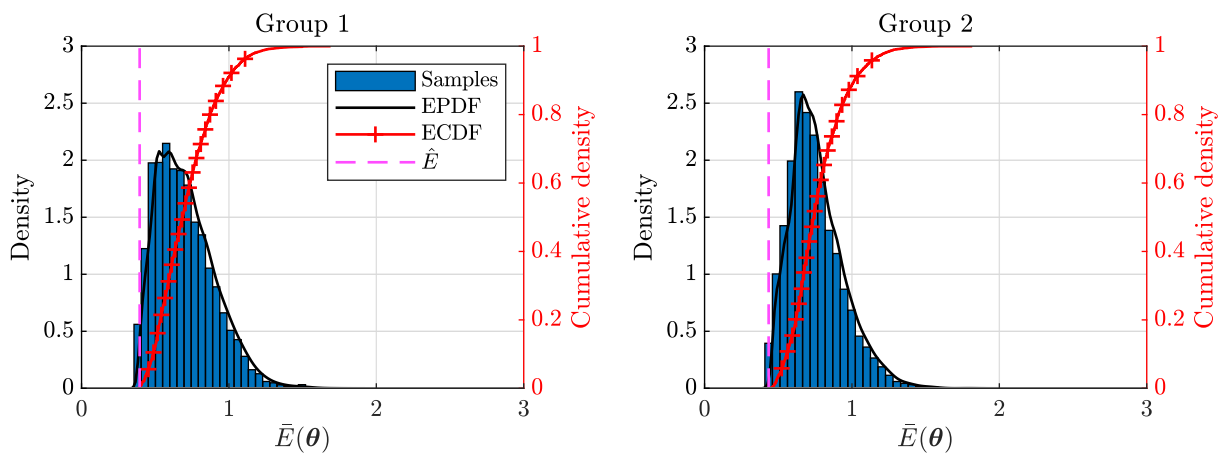
Finally, Figures 24 and 25 show some responses of the suggested model with uncertainties for Branch 1 and 4, respectively. Both Group 1 were considered to compare the responses from the same inputs  $C(t)$  and initial conditions  $A|_{t=0}$  used during the Bouc-Wen model calibration procedure. The responses of Branch 1 were the best estimation and the ones of Branch 4 the worst estimation scenario, where the error metric has its higher value.

Figure 20: Branch 1 - Distributions of the error metric: estimated probability density function (EPDF) and empirical cumulative distribution function (ECDF). The minimum values given by the CE method are  $\hat{E} = 0.3171$  (Group 1) and  $\hat{E} = 0.3655$  (Group 2).



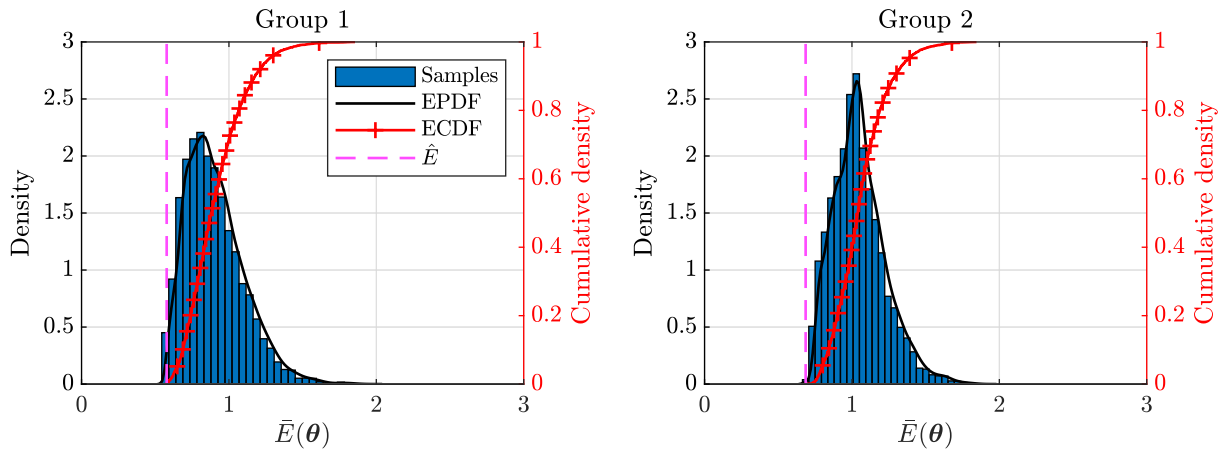
Source: Author's own elaboration.

Figure 21: Branch 2 – Distributions of the error metric: estimated probability density function (EPDF) and empirical cumulative distribution function (ECDF). The minimum values given by the CE method are  $\hat{E} = 0.3942$  (Group 1) and  $\hat{E} = 0.4347$  (Group 2).



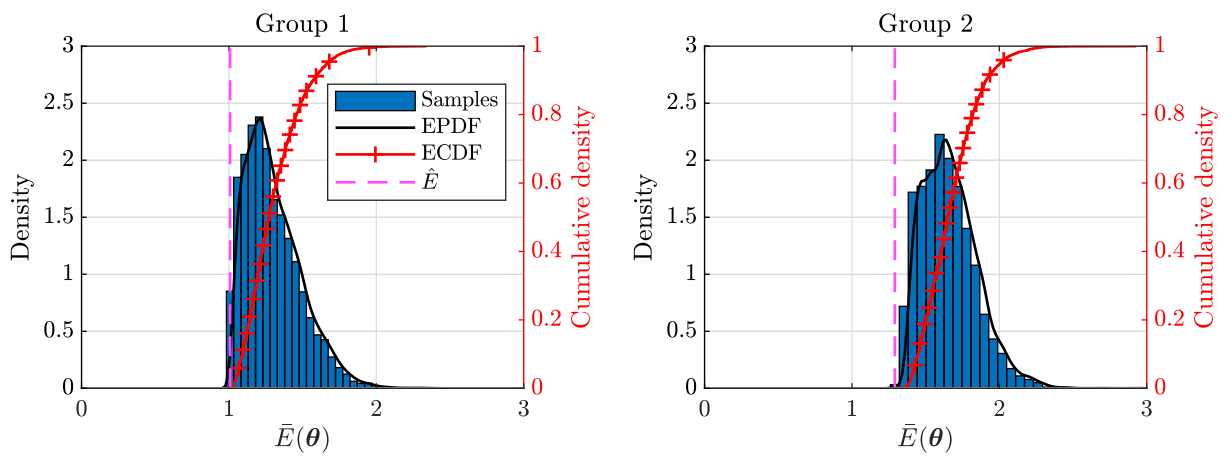
Source: Author's own elaboration.

Figure 22: Branch 3 – Distribution of the error metric: estimated probability density function (EPDF) and empirical cumulative distribution function (ECDF). The minimum values given by the CE method are  $\hat{E} = 0.5776$  (Group 1) and  $\hat{E} = 0.6857$  (Group 2).



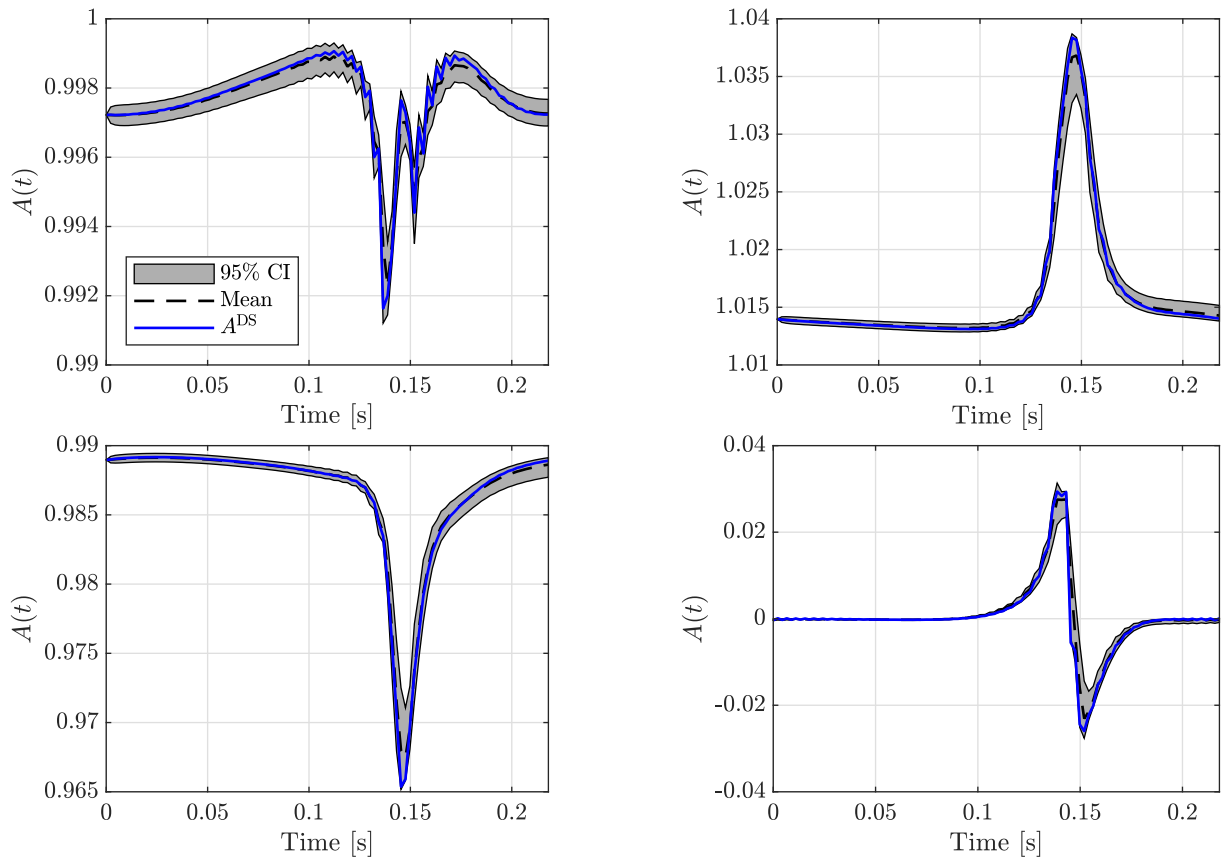
Source: Author's own elaboration.

Figure 23: Branch 4 – Distribution of the error metric: estimated probability density function (EPDF) and empirical cumulative distribution function (ECDF). The minimum values given by the CE method are  $\hat{E} = 1.0116$  (Group 1) and  $\hat{E} = 1.6672$  (Group 2).



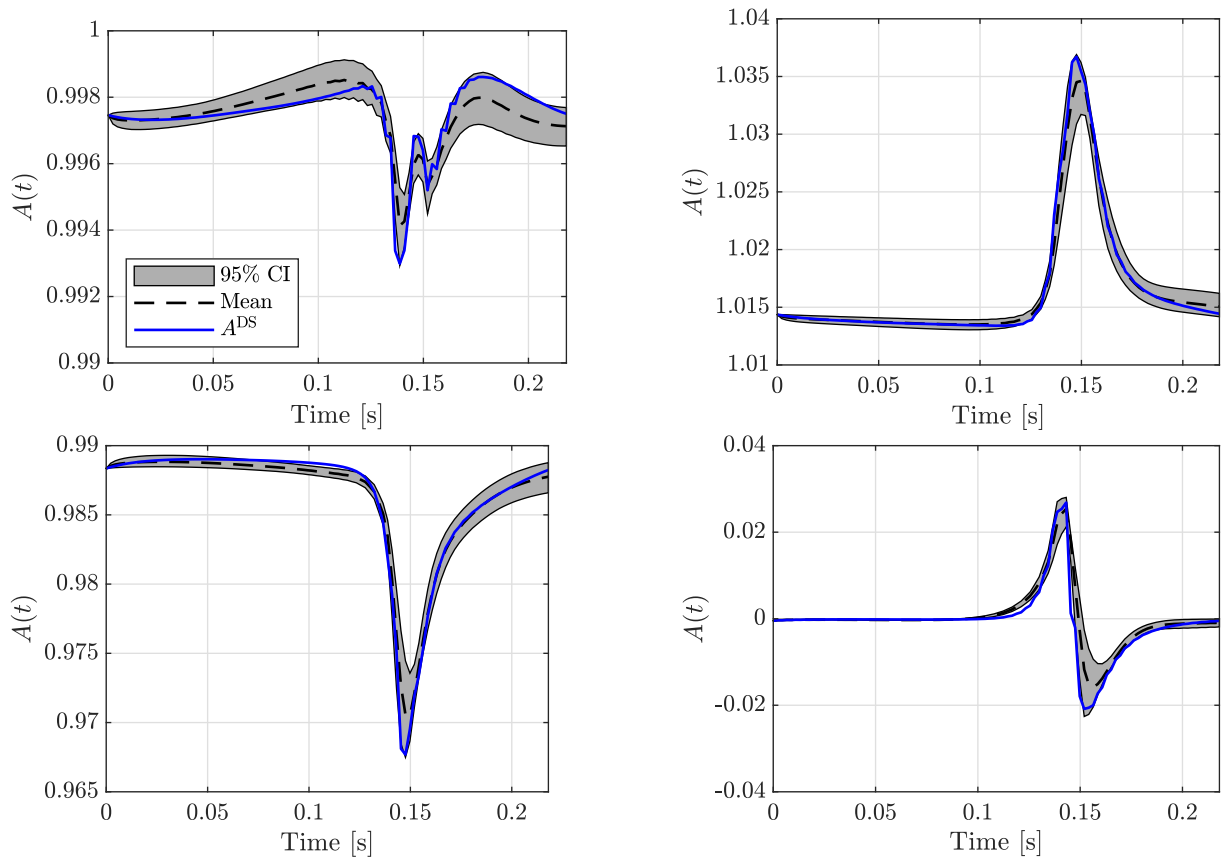
Source: Author's own elaboration.

Figure 24: Branch 1, Group 1 – Propagation of the uncertainties. Responses of the stochastic model: 95% confidence interval (CI), its mean (Mean) and corresponding viscoelastic internal variables from the dataset ( $A^{DS}$ ). Best Group 1 estimation scenario.



Source: Author's own elaboration.

Figure 25: Branch 4, Group 1 – Propagation of the uncertainties. Responses of the stochastic model: 95% confidence interval (CI), its mean (Mean) and corresponding viscoelastic internal variables from the dataset ( $A^{DS}$ ). Worst Group 1 estimation scenario.



Source: Author's own elaboration.

Tables 7 and 8 show the parameters of the CE method and of the Metropolis-Hastings algorithm. It is worth mentioning that the elapsed time of the Bayesian inference was one order of magnitude higher than the elapsed time of the CE method, and the absolute and relative tolerances adopted in the Runge-Kutta method were an important factor in the computation time: more lenient tolerances can reduce the elapsed time. These simulations were performed on a notebook with an Intel(R) Core(TM) i7-4510U CPU 2.00GHz processor.

Table 7: Cross-Entropy method. Elapsed time to estimate the values of the parameters of the Bouc-Wen model:  $N_s = 100$  samples,  $N_{\mathcal{E}} = 4$  samples,  $\epsilon_{\max} = 10^{-6}$ ,  $l_{\max} = 500$  iterations and  $a = 0.8$ .

Branch	Group	Time [min]
Branch 1	Group 1	63
	Group 2	39
Branch 2	Group 1	27
	Group 2	22
Branch 3	Group 1	35
	Group 2	26
Branch 4	Group 1	50
	Group 2	12

Source: Author's own elaboration.

Table 8: Bayesian inference. Elapsed time to estimate the values of the parameters of the Bouc-Wen model and the variance of the discrepancy:  $N_k = 2 \times 10^4$  samples.

Branch	Group	$\sigma^2$	$\bar{a}$ [%]	Time [min]
Branch 1	Group 1	0.09	43	311
	Group 2	0.07	43	172
Branch 2	Group 1	0.09	44	241
	Group 2	0.06	44	103
Branch 3	Group 1	0.09	46	149
	Group 2	0.07	44	83
Branch 4	Group 1	0.05	42	173
	Group 2	0.05	42	69

Source: Author's own elaboration.

Table 9 shows the estimated values of the parameters of the Bouc-Wen model and the variance of the discrepancy parameter in the Bayesian inference. Considering both the CE method and the maximum a posteriori (MAP) estimation<sup>4</sup>, there was a correspondence between the estimated values of parameters  $c$  and  $k$ . On the contrary, there was no

<sup>4</sup>The MAP estimation returns the set of parameters responsible for the highest probability of the posterior distribution. The MAP estimate and the Maximum Likelihood Estimate (MLE) are equivalent when noninformative prior distributions are adopted.

clear correspondence between the estimated values of parameters  $\alpha$  and  $\nu$ . It is worth mentioning that both estimators are equivalent for Branch 3, Group 2 and Branch 4, Group 2. This is because the MAP initial iteration receives the CE values, and throughout the Monte Carlo simulation, there was no other sample that generated a higher MAP value.

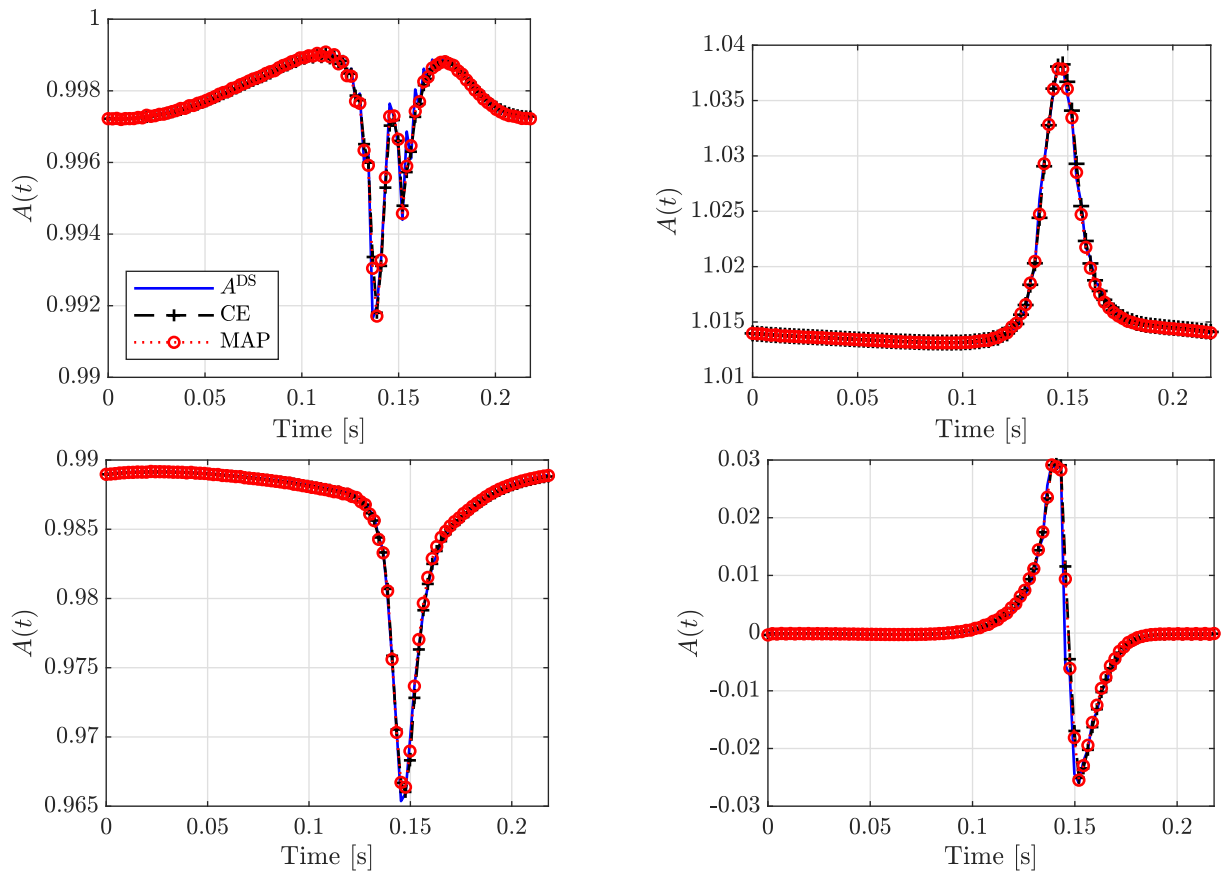
Table 9: Estimated values of the parameters of the Bouc-Wen model and the variance of the discrepancy.

Branch	Group	Estimator	$c$	$k$	$\alpha$	$\nu$	$\sigma_\epsilon^2$
Branch 1	Group 1	CE	0.0018	1.0000	0.1152	1.0220	n/a
		MAP	0.0016	1.0000	0.0227	2.0326	0.0062
	Group 2	CE	0.0035	1.0000	0.0418	1.8039	n/a
		MAP	0.0034	1.0000	0.0551	2.4126	0.0069
Branch 2	Group 1	CE	0.0020	1.0000	0.0194	1.5031	n/a
		MAP	0.0018	1.0001	0.1108	1.1788	0.0052
	Group 2	CE	0.0043	1.0000	0.0511	2.3418	n/a
		MAP	0.0042	1.0000	0.0433	2.1276	0.0040
Branch 3	Group 1	CE	0.0027	1.0000	0.1819	1.1381	n/a
		MAP	0.0027	1.0000	0.2068	1.1640	0.0016
	Group 2	CE	0.0072	1.0000	0.0738	1.9416	n/a
		MAP	0.0072	1.0000	0.0738	1.9416	0.0100
Branch 4	Group 1	CE	0.0049	1.0001	1.0411	1.0418	n/a
		MAP	0.0057	1.0001	0.6845	1.0911	0.0028
	Group 2	CE	0.0154	1.0000	0.1077	1.8369	n/a
		MAP	0.0154	1.0000	0.1077	1.8369	0.0100

Source: Author's own elaboration.

Figures 26 and 27 compare some examples of deterministic responses of viscoelastic internal variables. In them, the black dashed and marked (+) lines correspond to deterministic responses of the suggested model adopting CE parameter values from Table 9. In addition, the red dotted and marked ( $\circ$ ) lines correspond to deterministic responses of the proposed model adopting MAP parameter values. Despite the differences in the parameter values in Table 9, Figures 26 and 27 indicate that both estimators provide similar responses. That is verified for both Branch 1, the best Group 1 estimation scenario, and Branch 4, the worst Group 1 estimation scenario.

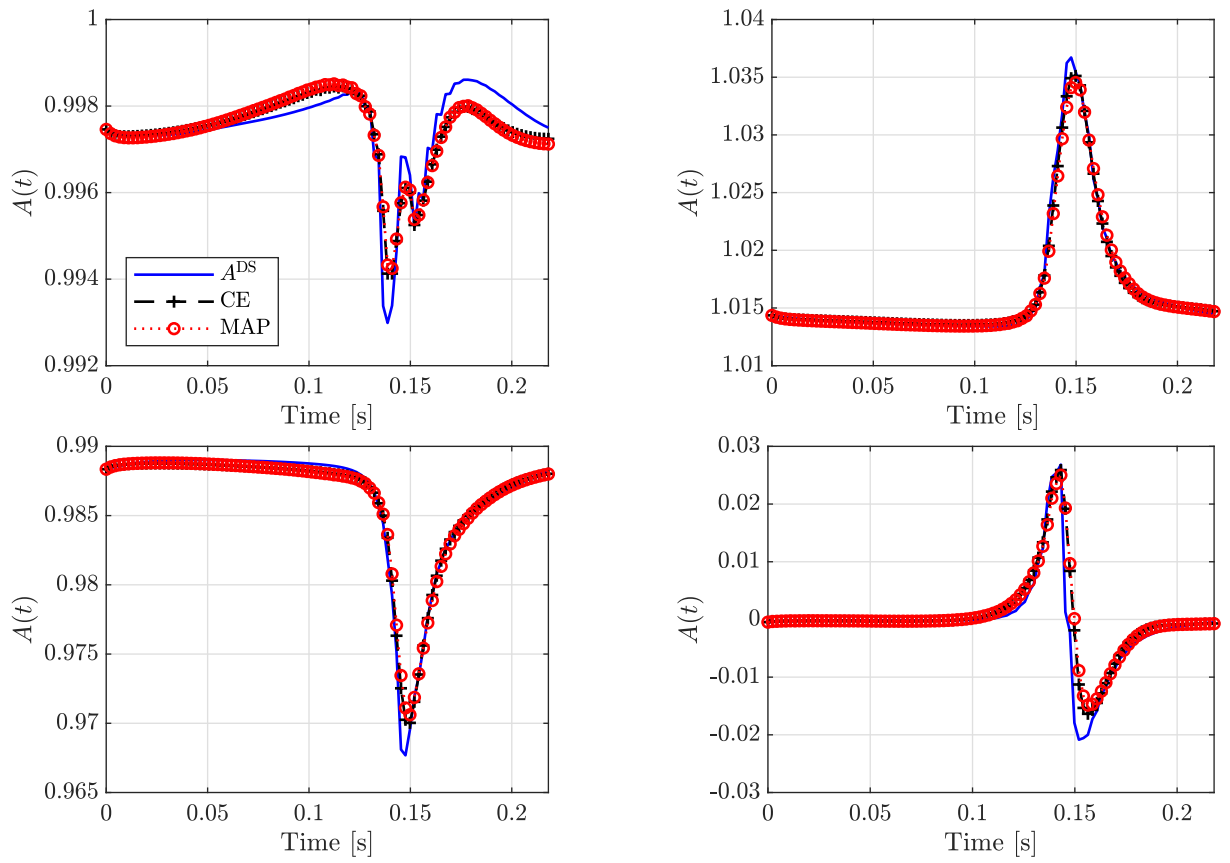
Figure 26: Branch 1, Group 1 – Deterministic responses of the Bouc-Wen model: CE method, MAP and corresponding viscoelastic internal variables from the dataset ( $A^{DS}$ ).



Source: Author's own elaboration.



Figure 27: Branch 4, Group 1 – Deterministic responses of the Bouc-Wen model: CE method, MAP and corresponding viscoelastic internal variables from the dataset ( $A^{\text{DS}}$ ).

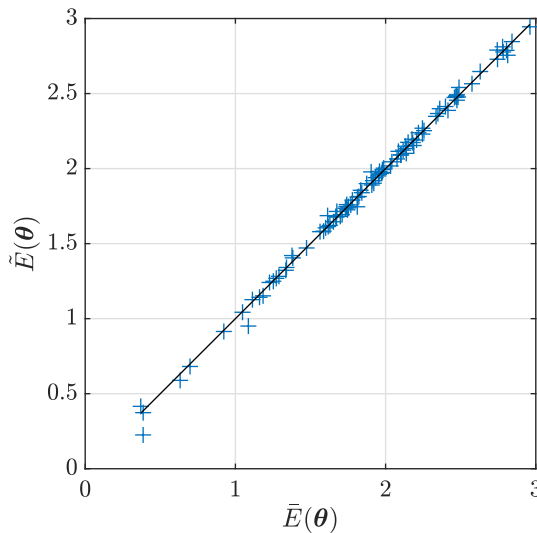


Source: Author's own elaboration.

### 3.2 PCE-BASED SURROGATE MODEL CALIBRATION

Both the UQLab Bayesian inference module (WAGNER *et al.*, 2022) and PCE module (MARELLI; LÜTHEN; SUDRET, 2022) were combined in this section to perform a Bayesian inference using a PCE-based surrogate model: a PCE-based surrogate model was built with univariate polynomials from the Uniform distributions in Table 4 and its coefficients were computed. As in the previous section, Figure 28 compares the error metrics  $\bar{E}(\boldsymbol{\theta})$  and  $\tilde{E}(\boldsymbol{\theta})$ . Table 10 contains additional information about the validation of the PCE-based surrogate model.

Figure 28: Bayesian inference using a PCE-based surrogate model. Branch 1, Group 1 – Comparison between error metrics  $\bar{E}(\boldsymbol{\theta})$  and  $\tilde{E}(\boldsymbol{\theta})$ . The disposition of the 100 cross-validation samples + indicates that the PCE-based surrogate model was adequate.



Source: Author's own elaboration.

Table 10: Bayesian inference using a PCE-based surrogate model. Validation of the PCE-based surrogate model.

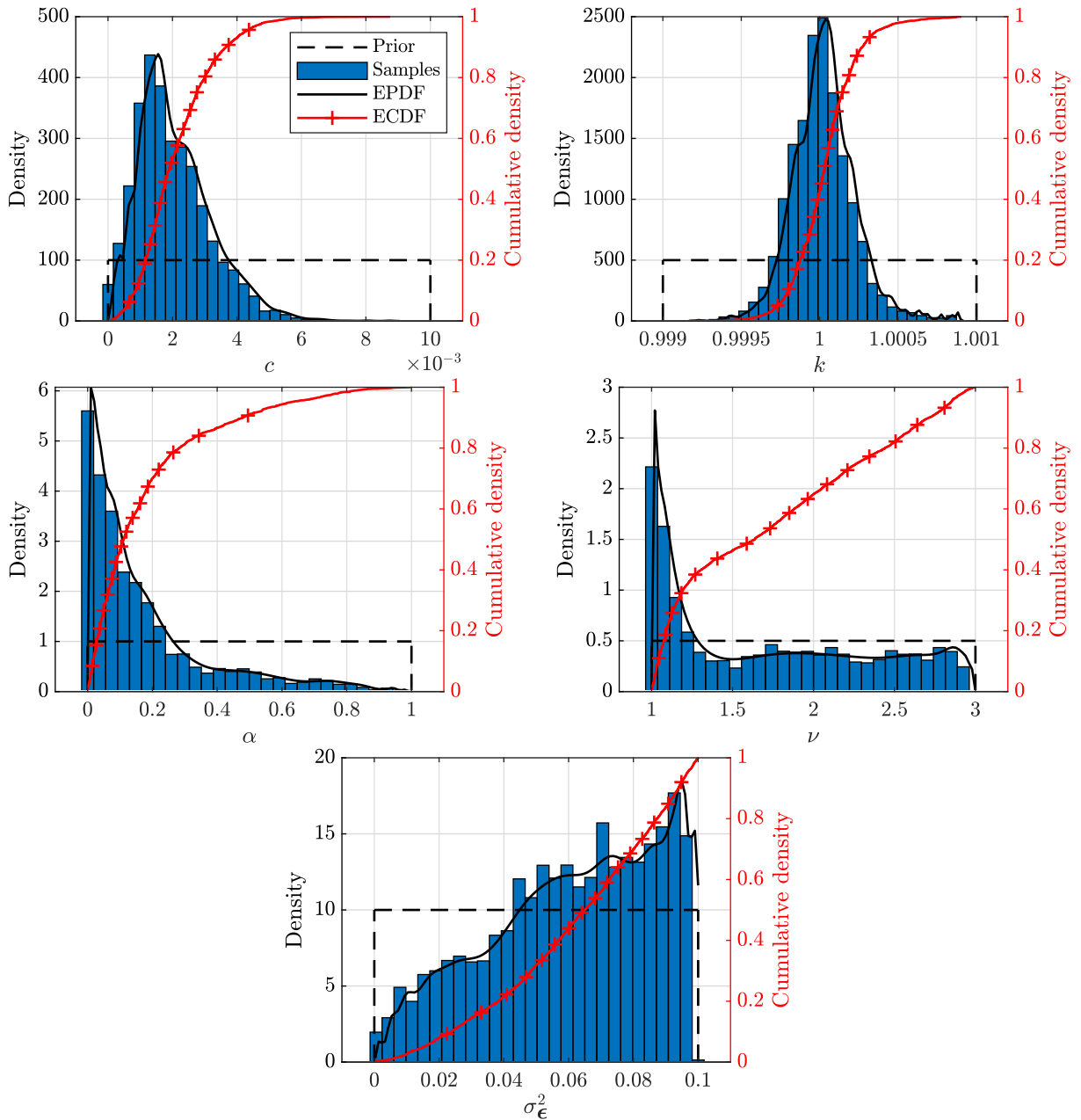
PCE degree	qNorm	Exp. Design	LOO error	Time [min]
13	0.75	1,000	$2.9 \cdot 10^{-3}$	12

Source: Author's own elaboration.

Information about the configuration of the Bayesian inference in UQLab is not addressed in this section, but the elapsed time to generate  $N_k = 2 \times 10^4$  samples was only 2 min. Figure 29 shows the densities and cumulative densities of the parameters of the Bouc-Wen model and of the variance of the discrepancy from the Bayesian inference using the PCE-based surrogate model: the continuous black line is the probability density estimates (EPDF) based on a normal kernel function, the black dashed line is the Uniform prior distribution, and the marked red line is the empirical cumulative distribution function (ECDF). From that, conclusions can be drawn:

- It was possible to calibrate the suggested model using the PCE-based surrogate model;
- The distributions of the parameters of the Bouc-Wen model and of the variance of the discrepancy parameter were close to the ones from the previous section;
- The total elapsed time from this procedure was 14 min. This correspond to a significant reduction compared to 311 min indicated in Table 8.

Figure 29: Bayesian inference using a PCE-based surrogate model. Branch 1, Group 1 – Distributions of the parameters of the Bouc-Wen model and variance of the discrepancy parameter: Uniform prior (Prior), estimated probability density functions (EPDF) and empirical cumulative distribution functions (ECDF).



Source: Author's own elaboration.

## 4 FINAL REMARKS

This chapter summarizes this work. It also addresses some points aiming to advance this research further.

---

### 4.1 SUMMARY

This work deals with creating simple models for simulating viscoelastic internal variables that describe the viscoelasticity in steady-state rolling tires. In order to archive this objective, Michelin furnished a dataset composed of components of right Cauchy-Green deformation tensors and viscoelastic internal variables. These data were generated from the finite element approximation of a steady-state rolling tire. The full-order model is based on a generalized Maxwell model, in which the branches of interest are defined according to the dynamic behavior of the viscoelastic internal variables.

The suggested model was formulated from this generalized Maxwell model: in a branch of interest, the component of the right Cauchy-Green deformation tensor was related to the corresponding viscoelastic internal variable and its time derivative by the series connection of a spring and a dashpot element. In addition, the hysteresis in the branch was considered through a hysteretic output given by the Bouc-Wen model. After algebraic manipulation, the suggested model was defined as a system of nonlinear differential equations solved numerically. After formulating the model, two procedures were defined:

- The first procedure consisted of visually analyzing the dataset to avoid redundant data. After this procedure, a reduced number of components of the right Cauchy-Green deformation tensors were selected and defined as inputs. These inputs were considered adequate to represent all components of the right Cauchy-Green deformation tensors of the dataset;
- The second procedure consisted of defining a model calibration strategy considering the inputs. Afterward, it was verified through numerical simulations that better results were obtained if each branch of interest was divided into two groups.

Concerning the calibration strategy, an error metric was defined to evaluate the discrepancies between the suggested model's response and data independent of the inputs' differences. Then, the calibration strategy was proposed based on:

1. Performing a global sensitivity analysis by evaluating Sobol's indices from the coefficients of a PCE-based surrogate model;
2. Obtaining the optimal set of influential parameters using the Cross-Entropy method;
3. Estimating the distributions of influential parameters through Bayesian inference.

After validating the PCE-based surrogate model, an evaluation of the Sobol indices indicates that some parameters of the Bouc-Wen model do not significantly influence the variability of the error metric. Therefore, these parameters were not considered in the later steps of the calibration strategy saving computational time.

The solution to the optimization problem obtained by minimizing the error metric offered preliminary information on the influential parameters of the Bouc-Wen model. In addition, the Cross-Entropy method resulted in the best forecast prediction of the Bouc-Wen model. By following an Uncertainty Quantification framework, the distributions of the influential parameters of the Bouc-Wen model were estimated using Bayesian inference. To be rigorous in performing Monte Carlo simulation, a procedure was established to guarantee the convergence of first and second central moments and the stability of the Markov Chain. These distributions were used to propagate the uncertainties through the error metric and responses of the suggested model. The same calibration strategy was adopted for each group of branches of interest, and some conclusions were drawn:

- Roughly, the distributions of the error metric allowed to define a response adequacy criterion: the models in which the error metric distributions are located after the unity do not adequately simulate the viscoelastic internal variables;
- The uncertainties were propagated through the responses of the suggested model. The responses were among the data for the first three branches of interest.

Despite some efforts related to the calibration strategy, the latter allows for creating a simple model that predicts the best-fitting viscoelastic internal variables. After this process, the suggested model was capable of simulating viscoelastic internal variables considering uncertainties with reduced computational cost. A robust and cheaper computational model facilitates numerical simulations and research to obtain more robust tires. For this reason, the results of this work also contribute to the advancement of research on computational models that are more robust and have a reduced computational cost.

## 4.2 PERSPECTIVES OF FUTURE WORK

Some points for further advancing this research are addressed as follows:

1. The selection procedure of the inputs (components of the right Cauchy-Green deformation tensors) and corresponding viscoelastic internal variables is based solely on visualizing the data. This topic deserves more attention because an excessive number of inputs does not necessarily improve the prediction. Moreover, it can make this procedure time-consuming. An optimum number of inputs is not defined;
2. The implemented MATLAB scripts can be improved to reduce the computation time. Notably, the use of narrower absolute and relative tolerances in the Runge-Kutta method is responsible for an increase in computation time;
3. In the adopted calibration strategy, a PCE-based surrogate model is already built for the global sensitivity analysis step. It can be interesting to perform the Bayesian inference not using the Bouc-Wen model but the PCE-based surrogate model because the latter possibly run faster during the Monte Carlo simulation. Partial results related to this item were briefly addressed;
4. The initial conditions of the viscoelastic internal variables can be considered random variables to be calibrated. Some constraints can be investigated to ensure equality between the distributions of the initial and final conditions of the viscoelastic internal variables. By doing so, the behavior of these variables is consistent with the cyclic motion of the steady-state rolling tire. It is important to respect this behavior if the present model is to substitute the viscoelastic internal variables of the finite element approximation;
5. The Bouc-Wen model on which the proposed model is based is phenomenological, and its parameters do not have a physical meaning. It can be interesting to adopt the same methodology in a further study using data of different finite element approximations, e.g., varying the material properties of the tire or varying dimensions. From this analysis, the suggested model may be correlated to variations of the tire properties and replace parts of the finite element model;
6. One of the advantages of this work is to obtain a simple and representative model considering hysteresis in tires by adopting a Bayesian framework. Although this work deals with steady-state rolling tire problems, the Bouc-Wen model and its parameter calibration strategy can be extended to other dynamic systems. The solutions in this work can be applied to problems that involve hysteresis and are computationally expensive to run with finite element models, such as jointed structures (TELOLI *et al.*, 2021; TELOLI *et al.*, 2022; MIGUEL; TELOLI; da Silva, 2022) and bit-rock interaction of a drill (REAL *et al.*, 2019).

### 4.3 CONTRIBUTIONS TO THE LITERATURE

Some results of this work are in the following manuscript under review:

- **Rafael da S. Raqueti**, Rafael de O. Teloli, Samuel da Silva, Philippe Bussetta, Americo Cunha Jr., "On the use of stochastic Bouc-Wen model for simulating viscoelastic internal variables from a finite element approximation of steady-rolling tire," *Journal of Vibration and Control*.



## References

- ALIZADEH, R.; ALLEN, J. K.; MISTREE, F. Managing computational complexity using surrogate models: a critical review. **Research in Engineering Design**, London, v. 31, n. 3, p. 275–298, apr 2020.
- BOER, P.-T. de; KROESE, D. P.; MANNOR, S.; RUBINSTEIN, R. Y. A tutorial on the cross-entropy method. **Annals of Operations Research**, New York, v. 134, n. 1, p. 19–67, feb 2005.
- BOTEV, Z. I. The normal law under linear restrictions: simulation and estimation via minimax tilting. **Journal of the Royal Statistical Society: Series B (Statistical Methodology)**, Chichester, v. 79, n. 1, p. 125–148, feb 2016.
- BRANCATI, R.; STRANO, S.; TIMPONE, F. An analytical model of dissipated viscous and hysteretic energy due to interaction forces in a pneumatic tire: Theory and experiments. **Mechanical Systems and Signal Processing**, London, v. 25, n. 7, p. 2785–2795, oct 2011.
- CRESTAUX, T.; MAÎTRE, O. L.; MARTINEZ, J.-M. Polynomial chaos expansion for sensitivity analysis. **Reliability Engineering & System Safety**, London, v. 94, n. 7, p. 1161–1172, jul 2009.
- CUNHA, A. Enhancing the performance of a bistable energy harvesting device via the cross-entropy method. **Nonlinear Dynamics**, Dordrecht, v. 103, n. 1, p. 137–155, 2021.
- DANTAS, E.; JR, A. C.; SOEIRO, F.; CAYRES, B.; WEBER, H. An inverse problem via cross-entropy method for calibration of a drill string torsional dynamic model. In: **25th ABCM International Congress on Mechanical Engineering (COBEM 2019)**. [S.l.: s.n.], 2019.
- FANCELLO, E.; PONTHOT, J.-P.; STAINIER, L. A variational formulation of constitutive models and updates in non-linear finite viscoelasticity. **International Journal for Numerical Methods in Engineering**, Oxford, v. 65, n. 11, p. 1831–1864, 2006.
- GELMAN, A.; CARLIN, J. B.; STERN, H. S.; RUBIN, D. B.; DUNSON, D. B. **Bayesian Data Analysis**. [S.l.]: Taylor Francis Ltd., 2013. ISBN 1439898200.
- GHANEM, P. D. S. R. G. **Stochastic Finite Elements: A Spectral Approach**. [S.l.]: Springer New York, 2011. ISBN 1461277957.
- GHOREYSHI, M. H. R. A State Of The Art Review Of The Finite Element Modelling Of Rolling Tyres. **Iranian Polymer Journal (English)**, Heidelberg, v. 17, n. 8, p. 571–597, 2008.
- HALL, D. E.; MORELAND, J. C. Fundamentals of Rolling Resistance. **Rubber Chemistry and Technology**, Akron, v. 74, n. 3, p. 525–539, jul 2001.

- HOMMA, T.; SALTELLI, A. Importance measures in global sensitivity analysis of nonlinear models. **Reliability Engineering & System Safety**, London, v. 52, n. 1, p. 1–17, apr 1996.
- HYNDMAN, R. J.; KOEHLER, A. B. Another look at measures of forecast accuracy. **International Journal of Forecasting**, Amsterdam, v. 22, n. 4, p. 679–688, oct 2006.
- ISMAIL, M.; IKHOUANE, F.; RODELLAR, J. The Hysteresis Bouc-Wen Model, a Survey. **Archives of Computational Methods in Engineering**, Dordrecht, v. 16, n. 2, p. 161–188, feb 2009.
- KROESE, D. P.; RUBINSTEIN, R. Y.; GLYNN, P. W. The Cross-Entropy Method for Estimation. In: **Handbook of Statistics - Machine Learning: Theory and Applications**. [S.l.]: Elsevier, 2013. p. 19–34.
- KROESE, D. P.; TAIMRE, T.; BOTEV, Z. I. **Handbook of Monte Carlo Methods**. [S.l.]: Wiley, 2011.
- LIU, C. H.; HOFSTETTER, G.; MANG, H. A. 3D finite element analysis of rubber-like materials at finite strains. **Engineering Computations**, Bingley, v. 11, n. 2, p. 111–128, feb 1994.
- MARELLI, S.; LAMAS, C.; KONAKLI, K.; MYLONAS, C.; WIEDERKEHR, P.; SUDRET, B. **UQLab user manual – Sensitivity analysis**. [S.l.], 2022. Report UQLab-V2.0-106.
- MARELLI, S.; LÜTHEN, N.; SUDRET, B. **UQLab user manual – Polynomial chaos expansions**. [S.l.], 2022. Report UQLab-V2.0-104.
- MARELLI, S.; SUDRET, B. UQLab: A Framework for Uncertainty Quantification in Matlab. In: **Vulnerability, Uncertainty, and Risk**. [S.l.]: American Society of Civil Engineers, 2014.
- MIGUEL, L. P.; TELOLI, R. O.; da Silva, S. Bayesian model identification through Harmonic Balance Method for hysteresis prediction in bolted joints. **Nonlinear Dynamics**, Dordrecht, v. 107, n. 1, p. 77–98, 2022. ISSN 1573-269X.
- OROUMIYEH, F.; ZHU, Y. Brake and tire particles measured from on-road vehicles: Effects of vehicle mass and braking intensity. **Atmospheric Environment: X**, Oxford, v. 12, p. 100121, dec 2021.
- PACEJKA, H. **Tire and Vehicle Dynamics**. 3rd. ed. [S.l.]: Elsevier Science Technology, 2012. ISBN 0080970168.
- PALAR, P. S.; ZUHAL, L. R.; SHIMOYAMA, K.; TSUCHIYA, T. Global sensitivity analysis via multi-fidelity polynomial chaos expansion. **Reliability Engineering & System Safety**, London, v. 170, p. 175–190, feb 2018.
- REAL, F. F.; BATOU, A.; RITTO, T. G.; DESCELIERS, C. Stochastic modeling for hysteretic bit–rock interaction of a drill string under torsional vibrations. **Journal of Vibration and Control**, London, v. 25, n. 10, p. 1663–1672, 2019.

- RUBINSTEIN, R. Y.; KROESE, D. P. **The Cross-Entropy Method**. [S.l.]: Springer New York, 2011. ISBN 1441919406.
- SAADI, H. A.; YKHLEF, F.; GUESSOUM, A. MCMC for parameters estimation by Bayesian approach. In: **Eighth International Multi-Conference on Systems, Signals & Devices**. [S.l.]: IEEE, 2011.
- SEGALMAN, D. J. A Four-Parameter Iwan Model for Lap-Type Joints. **Journal of Applied Mechanics**, Tehran, v. 72, n. 5, p. 752–760, 02 2005. ISSN 0021-8936.
- SOBOL, I. M. Sensitivity estimates for nonlinear mathematical models. **Mathematical and Computer Modelling**, Kidlington, v. 1, p. 407–414, 1993.
- SOIZE, C. **Uncertainty Quantification**. [S.l.]: Springer-Verlag GmbH, 2017. ISBN 3319543385.
- SUDRET, B. Global sensitivity analysis using polynomial chaos expansions. **Reliability Engineering & System Safety**, Elsevier BV, v. 93, n. 7, p. 964–979, jul 2008.
- SULLIVAN, C. C.; YAMASHITA, H.; SUGIYAMA, H. Reduced Order Modeling of Deformable Tire-Soil Interaction With Proper Orthogonal Decomposition. **Journal of Computational and Nonlinear Dynamics**, New York, v. 17, n. 5, mar 2022.
- TALLEC, P. L.; RAHLER, C. Numerical models of steady rolling for non-linear viscoelastic structures in finite deformations. **International Journal for Numerical Methods in Engineering**, Oxford, v. 37, n. 7, p. 1159–1186, apr 1994.
- TELOLI, R. O.; BUTAUD, P.; CHEVALLIER, G.; da Silva, S. Good practices for designing and experimental testing of dynamically excited jointed structures: The Orion beam. **Mechanical Systems and Signal Processing**, London, v. 163, p. 108172, 2022. ISSN 0888-3270.
- TELOLI, R. O.; da Silva, S.; RITTO, T. G.; CHEVALLIER, G. Bayesian model identification of higher-order frequency response functions for structures assembled by bolted joints. **Mechanical Systems and Signal Processing**, London, v. 151, p. 107333, 2021. ISSN 0888-3270.
- TONEGAWA, Y.; SASAKI, S. Development of tire-wear particle emission measurements for passenger vehicles. **Emission Control Science and Technology**, Springer, v. 7, n. 1, p. 56–62, 2021.
- WAGNER, P.-R.; NAGEL, J.; MARELLI, S.; SUDRET, B. **UQLab user manual – Bayesian inversion for model calibration and validation**. [S.l.], 2022. Report UQLab-V2.0-113.
- WALTER, J. D.; CONANT, F. S. Energy Losses in Tires. **Tire Science and Technology**, The Tire Society, v. 2, n. 4, p. 235–260, nov 1974.
- WIENER, N. The homogeneous chaos. **American Journal of Mathematics**, Baltimore, v. 60, n. 4, p. 897–936, 1938.